



Insights into mantle-type volatiles contribution from dissolved gases in artesian waters of the Great Artesian Basin, Australia



F. Italiano ^{a,*}, G. Yuce ^{b,c,d}, I.T. Uysal ^b, M. Gasparon ^{b,e,f}, G. Morelli ^e

^a Istituto Nazionale di Geofisica e Vulcanologia, sezione di Palermo, Italy

^b The Queensland Geothermal Energy Centre of Excellence, The University of Queensland, QLD, Australia

^c Eskisehir Osmangazi University, Department of Geological Engineering, Meselik, Turkey

^d Hacettepe University, Department of Geological Engineering, Beytepe, Ankara, Turkey

^e School of Earth Sciences, The University of Queensland, QLD, Australia

^f Australian National Centre for Groundwater Research and Training, Australia

ARTICLE INFO

Article history:

Received 8 August 2013

Received in revised form 15 April 2014

Accepted 17 April 2014

Available online 29 April 2014

Editor: David R. Hilton

Keywords:

Dissolved gas geochemistry

Great Artesian Basin

Mantle

Fluids

Tectonic structures

ABSTRACT

The geochemical features of the volatiles dissolved in artesian thermal waters discharged over three basins (Millungera, Galilee and Cooper basin) of the Australian Great Artesian Basin (GAB) consistently indicate the presence of fluids from multiple gas sources located in the crust (e.g. sediments, oil reservoirs, granites) as well as minor but detectable contributions of mantle/magma-derived fluids. The gases extracted from 19 water samples and analyzed for their chemical and isotopic composition exhibit amounts of CO₂ up to about 340 mlSTP/L_{H₂O} marked by a $\delta^{13}\text{C}_{\text{TDC}}$ (Total Dissolved Carbon) ranging from -16.9 to $+0.18\%$ vs PDB, while CH₄ concentrations vary from 4.4×10^{-5} to 4.9 mlSTP/L_{H₂O}. Helium contents were between 9 and >2800 times higher than equilibrium with Air Saturated Water (ASW), with a maximum value of 0.12 mlSTP/L_{H₂O}. Helium isotopic composition was in the 0.02–0.21 Ra range (Ra = air-normalized ³He/⁴He ratio). The three investigated basins differ from each other in terms of both chemical composition and isotopic signatures of the dissolved gases whose origin is attributed to both mantle and crustal volatiles. Mantle He is present in the west-central and hottest part of the GAB despite no evidence of recent volcanism. We found that the partial pressure of helium, significantly higher in crustal fluids than in mantle-type volatiles, enhances the crustal He signature in the dissolved gases, thus masking the original mantle contribution. Neotectonic activity involving deep lithospheric structures and magma intrusions, highlighted by recent geophysical investigations, is considered to be the drivers of mantle/magmatic volatiles towards the surface. The results, although pertaining to artesian waters from a vast area of >542,000 km², provide new constraints on volatile injection, and show that fluids' geochemistry can provide additional and independent information on the geo-tectonic settings of the Great Artesian Basin and its geothermal potential.

© 2014 Elsevier B.V. All rights reserved.

1. Introduction

The Great Artesian Basin (GAB) of Australia is unique not only because it is the largest and deepest artesian basin in the world, but also because it experiences conspicuously elevated crustal and mantle degassing in association with high heat production (Torgersen et al., 1992; Habermehl and Pestov, 2002). Highly radioactive crust in the central-western part of the GAB is responsible for an increase in heat flow and regional ⁴He flux, whereas the reduced heat flow with enhanced ³He flux is attributed to young volcanism in its eastern part (Sass and Lachenbruch, 1978; Torgersen and Clarke, 1985; Duncan and McDougall, 1989; Torgersen et al., 1992; Bethke et al., 1999). Eastern Australia has been the site of both hotspot volcanism and intraplate

lava flow fields since the late Cretaceous (Wellman and McDougal, 1974). Hotspot volcanism occurs as a response to the northward migration of Australia away from Antarctica, and is currently centred in Bass Strait in southeast Australia. Intraplate lava flow fields are distributed across the east coast in time and space, but the most recent activity (<5 Ma) is concentrated in northeast Queensland and southern Victoria (Johnson, 1989; Vasconcelos et al., 2008). A ³He-rich gas component indicating a mantle contribution of up to 7% in the GAB groundwater was observed at localities (at $\sim 20.5^\circ \text{S } 144^\circ \text{E}$, $\sim 25.5^\circ \text{S } 146^\circ \text{E}$, and $\sim 27^\circ \text{S } 144.5^\circ \text{E}$) in close proximity to Cenozoic lava flow fields (Torgersen et al., 1987; Torgersen et al., 1992), however to date there has been no evidence suggesting a mantle helium input to the groundwater further west, in the central and hottest part of the GAB. Natural gases from the Eromanga and Cooper Basins underlying the central-western part of the GAB, however, have extremely high CO₂ contents of more than 50%, although gases from most Australian basins

* Corresponding author. Tel.: +39 0916809411.

E-mail address: francesco.italiano@ingv.it (F. Italiano).

contain CO₂ of <5% (Boreham et al., 2001). Gases with CO₂ contents >5% in association with narrowly ranging $\delta^{13}\text{C}$ values between -3 and -10‰ in the Eromanga and Cooper Basins are considered to be originated from a mantle source (Boreham et al., 2001). Although no surface manifestation of volcanic activity is present in this region, it has been demonstrated elsewhere that mantle volatiles can be transferred into the shallow crust following extensional tectonic activity (Oxburgh and O'Nions, 1987; Kennedy and van Soest, 2006; Banerjee et al., 2011). The injection of mantle-derived fluids into geothermal reservoirs and groundwaters can be detected by using the He isotope geochemistry of volatiles even in regions where there is no active volcanism (e.g., Italiano et al., 2000; Güleç et al., 2002; Kulongoski et al., 2005; Italiano et al., 2013). The aims of this article are to evaluate the chemical and isotopic composition of the whole gas phase dissolved in deep artesian waters to explore whether a mantle fluid flux occurs in the central part of the GAB, and to discuss implications for active tectonics, and heat source and geothermal potential in the central GAB. A broad scale survey was conducted to collect gases dissolved in artesian thermal waters throughout the Galilee and Millungera Basins, and the northern part of the Cooper Basin in SW Queensland (Fig. 1). Water samples were taken from 19 deep artesian wells mostly in areas that have not been sampled by previous investigators (Torgersen et al.,

1987; Torgersen et al., 1992), and analyzed for dissolved gas contents (He, CO₂, CH₄, N₂ and O₂), and He, Ar and C isotopes.

2. Geological background and hydrology

The GAB comprises the Mesozoic Eromanga, Surat and Carpentaria Basins and parts of the Permian Bowen and Galilee Basins (Habermehl, 2001, and references therein). The confined aquifers occur in quartzose sandstones of continental origin and mostly Triassic, Jurassic and Cretaceous ages. The most productive aquifers in the GAB are the Lower Cretaceous–Jurassic sequences, with about 500–1500 mg/L total dissolved solids and bore yields over 5 L/s. A thick Early Cretaceous argillaceous sequence of marine origin is the main confining unit. The groundwater recharge zone is located primarily along the eastern margin of the basin, and the large-scale regional groundwater flow direction is from the east towards the southwest.

The geology of the GAB consists of several broad synclinal structures trending north and northeast, overlying sedimentary, metamorphic and igneous rocks of pre-Jurassic or pre-Triassic ages. The Mesozoic sedimentary sequence in the central part of the basin reaches a maximum total thickness of about 3000 m (Habermehl, 2001). Parts of the

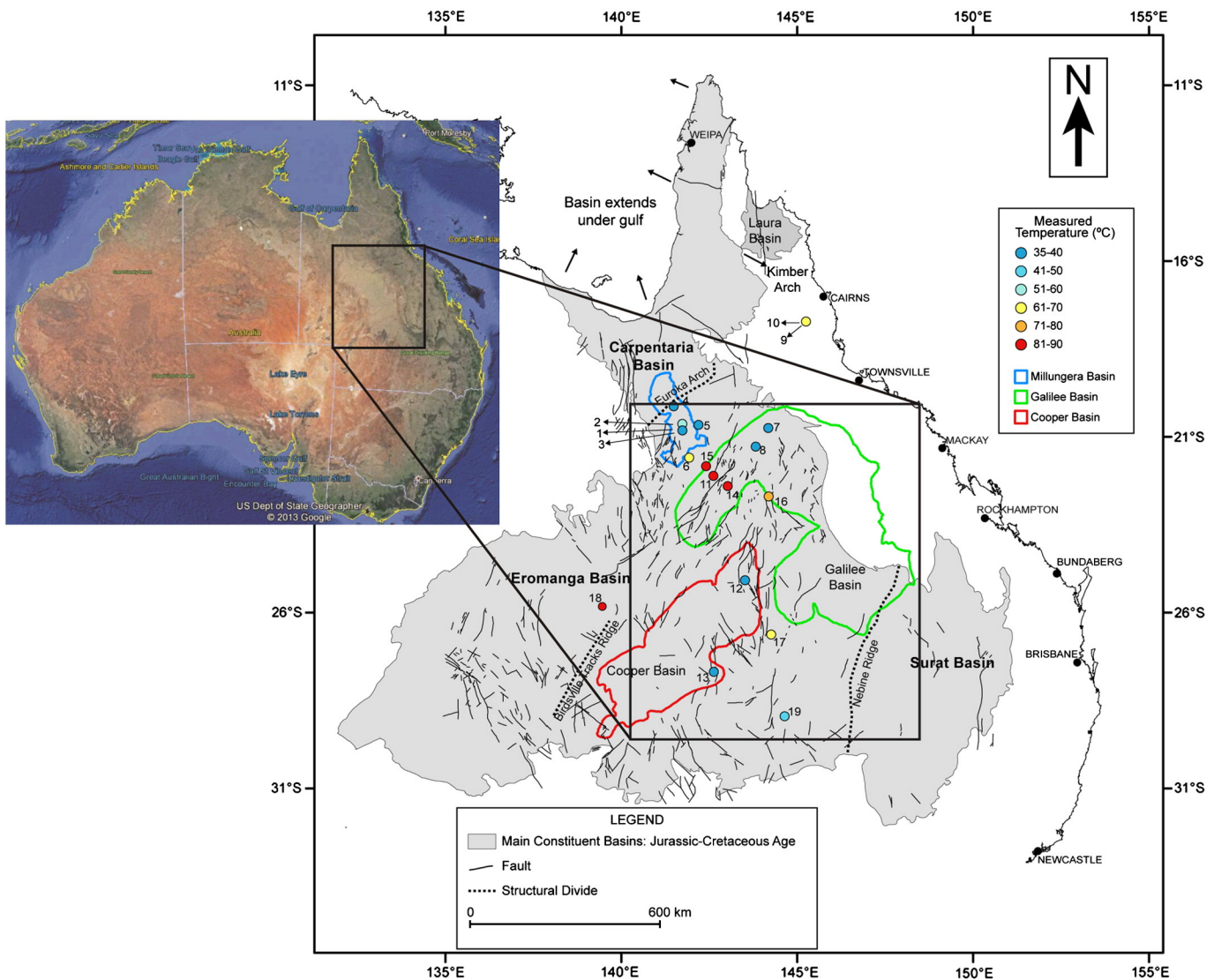


Fig. 1. Sample locations over the investigated Millungera, Galilee and Cooper Basins. The sampling sites are spread over an area marked by significant heat-flow anomalies (after OzTemp-Interpreted Temperature at 5 km depth, Commonwealth of Australia – Geoscience Australia, 2010). Sample ID shown as open circles in various colours compatible with water temperatures at the well head (see legend). (For interpretation of the references to colour in this figure legend, the reader is referred to the web version of this article.)

marginal areas of the basin have been eroded, in particular along the eastern border, which was uplifted during Cainozoic times. Several major fault and fold systems occur in the basin, in places forming en-echelon structures. The Eromanga Basin sequence was deformed during the mid-Tertiary by relatively mild northeast-southwest compression (Langford et al., 1995). Faulting reactivation caused a significant displacement in the Eromanga Basin sequence, locally reaching 780 m (Radke et al., 2000) during the last 95 Ma (Jones and Veevers, 1983; Wellman, 1987). Evidence for neotectonic activity in the GAB has been reported for the Lake Eyre region in northern South Australia, where Miocene-age sediments are clearly (Meixner et al., 2000) deformed. These include deformed bedding planes, small-scale folds, faults and fracture systems reflecting consistent Miocene and younger tectonic activity in central Australia (Waclawik et al., 2008).

The densely faulted basement of the Galilee basin is overlaid with the Upper Carboniferous–Lower Permian Joe Group, which is composed of quartzose sandstone and minor conglomerate with argillaceous beds. The uppermost unit of the Galilee Basin contains conglomerate, micaceous lithic sandstone and micaceous siltstone (Triassic Moolayember Formation). The basin overlies a crystalline basement that is step-faulted with downthrows to the west. The NE-trend is constrained by the Warrego Fault, with the Pleasant Creek Arch (a fault-bend anticline) as its southern boundary. Folding occurred during the deposition in the Galilee Basin. The Lovelle Depression, a shallower through, is located along the northwestern margin of the Galilee Basin. The Canaway Fault, the main normal fault in the GAB, separates the Galilee from the Cooper and the Warbuton Basins, which extend from south-east Queensland into north-west South Australia.

The Cooper Basin comprises a ~2 km-thick sequence of late Carboniferous and Permian glacial deposits (Merimellia and Tirrawarra Formations), deformed along NE-SW tectonic ridges (Gidgealpa–Merrimelia–Yanapurra ridges) and separated by paleo-depressions (Patchawarra, Nappamerri, Allunga and Tenappera troughs; PIRSA 2010). It hosts major geothermal, oil and gas deposits (Chopra, 2003; Wyborn et al., 2004; Radke, 2009). The Cooper Basin is overlaid by the 3 km-thick Mesozoic sequence of the Eromanga Basin.

The Millungera Basin, which is completely covered by a thin succession of sediments of the Jurassic–Cretaceous Eromanga–Carpentaria Basin, has been recently discovered based on the interpretation of aeromagnetic data and deep seismic reflection surveys (Korsch et al., 2011).

There are about 4700 flowing artesian and 20,000 non-flowing artesian water wells in the GAB, with further 3500 petroleum exploration

and production wells. The depth of the water wells ranges from a few hundred metres to almost 4 km.

3. Sampling and analytical procedures

In order to gain insight into the gas phases released over the GAB, we sampled 19 thermal waters (outlet temperatures ranging between 35 and 87 °C) from free-flowing artesian wells in November–December 2011 (Table 1), since no venting or bubbling gases are known to occur over the studied basins (Galilee, Millungera and Cooper). Some of the artesian waters have already been considered for their helium (Torgersen et al., 1992) and carbon (Boreham et al., 2001) isotopic systematics, but the composition of the dissolved gases has been obtained for the first time in this study. Our samples, collected specifically for the extraction of the whole gas phase for chemical and isotopic analyses, were stored in 240 ml pyrex bottles sealed in the field using rubber/teflon septa and purpose-built pliers, and analyzed within 1 month. Details of the sampling methodology are reported in Italiano et al. (2009, 2013) and further information on its suitability for both chemical and helium isotopic analysis is reported in Appendix A. The depth of the sampled bores ranged from 183 to 3903 m (Table 1). Only wells with the screen close to the base of the bore were sampled, to ensure that the water sampled at the surface was representative of the deep groundwater, and therefore that mixing with the shallower fluids would be minimized.

In the laboratory, the dissolved gases were extracted after equilibrium was reached at constant temperature with a host-gas (high-purity argon) injected in the sample bottle (for further details see Italiano et al., 2009, 2013). Chemical analyses were carried out by gas-chromatography (Perkin Elmer Clarus500 equipped with a double TCD-FID detector) using argon as the carrier gas. Typical uncertainties were within ±5%.

Helium isotope analyses were carried out on gas fractions extracted following the same procedure or, alternatively, on the already exsolved gas phase, and purified following methods described in the literature (Sano and Wakita, 1988; Hilton 1996; Italiano et al., 2001). The isotopic analyses of the purified helium were performed by using a static vacuum mass spectrometer (GVI5400TFT) that allows the simultaneous detection of ³He and ⁴He ion beams, thereby keeping the ³He/⁴He error of measurement to very low values. Typical uncertainties in the range of low-³He samples are within ±2%.

The isotopic composition of carbon from total dissolved carbon ($\delta^{13}\text{C}_{\text{TDC}}$) was measured on 2 ml of water sample introduced in

Table 1

Field data, location and basin indication of the investigated bores. Basins labels: M = Millungera; G = Galilee; C = Cooper. Samples from Innot hot springs are not attributed to any basin. Depth is the depth of the base of the screened well section (based on the available information). Coordinates according to the WGS84 Datum. EC = electrical conductivity in $\mu\text{S}/\text{cm}$. ORP = oxidation reduction potential in mV.

Basin	Sample ID	Sampling site	Date	Depth (m)	Longitude	Latitude	pH	T (°C)	EC ($\mu\text{S}/\text{cm}$)	ORP (mV)
M	1	Julia Creek/Longford Plains	13/12/2011	361	20° 48'31.41	141° 44'22.61	7.50	47.0	612	−128
M	2	Julia Creek/Railway	13/12/2011	360	20° 39'40.51	141° 44'45.91	7.60	49.1	640	−170
M	3	Julia Creek/Scare-bore	14/12/2011	344	20° 39'45.31	141° 43'09.11	8.00	56.0	641	−60
M	4	Julia Creek/Cabanda	14/12/2011	339	20° 07'06.81	141° 30'54.11	8.00	45.1	614	−162
M	5	Julia Creek/Nelie	14/12/2011	396	20° 39'23.2	142° 12'54.71	7.90	46.0	493	−57
M	6	Kynuna bore	14/12/2011	677	21° 34'36.40	141° 54'47.51	7.50	62.5	645	−200
G	7	Hughenden Shire-bore	15/12/2011	183	20° 50'51.11	144° 11'06.21	8.30	34.5	906	−90
G	8	Hughenden/Stamford	15/12/2011	565	21° 16'10.2	143° 48'32.11	8.70	43.0	455	−76
G	11	Weston	10/11/2011	1213	22° 06'31.5"	142° 37'29.7"	7.30	84.0	760	−30
G	14	Winton Town Bore	11/11/2011	1222	22° 23'12.7"	143° 02'50.3"	7.90	86.0	812	−27
G	15	Nuken/Winton	10/11/2011	1162	21° 51'36.3"	142° 25'18.8"	6.80	85.0	817	101
G	16	Greenhills/Longreach	09/11/2011	1000	22° 40'30.5"	144° 11'27.6"	8.10	75.0	840	−32
G	17	Quilpie Town Bore	04/11/2011	1200	26° 37'06.4"	144° 16'26.1"	8.10	61.0	1400	−101
C	12	Bonnie Doon/Jundah	06/11/2011	3903	25° 03'31"	143° 32'29"	6.10	41.8	6390	−111
C	13	Nockatunga/Nocconda	04/11/2011	1514	27° 39'55"	142° 38'55"	7.10	50.0	2244	−70
C	18	Birdsville	08/11/2011	1221	25° 51'44"	139° 28'22"	7.70	87.0	1200	−2
C	19	Yowah	05/11/2011	691	27° 58'23.1"	144° 38'10.8"	7.90	57.0	992	−57
	9	Innot Hot Spring/bore	16/12/2011	15	17° 40'1.50	145° 14'16.31	7.20	66.2	1041	235
	10	Innot Hot Spring	16/12/2011	Spring	17° 40'1.50	145° 14'19.21	7.98	68.6	1052	235

containers where high purity helium was injected to remove atmospheric CO₂. The water samples were acidified with phosphorus pentoxide in an auto-sampler to ensure complete release of CO₂ from acidified waters. CO₂ was then directly admitted to a continuous flow mass spectrometer (AP2003). The extracted CO₂ amounts represent the total content of dissolved carbon (TDC). The results are reported in δ‰ units relative to the V-PDB (Vienna–Pee Dee Belemnite) international standard. Standard deviation of the ¹³C/¹²C ratio was ±0.2‰.

Argon isotopes were measured by a multi-collector noble gas mass spectrometer (ARGUS, GVI) specifically designed for simultaneous measurement of ⁴⁰Ar, ³⁸Ar and ³⁶Ar isotopes using a detector that holds five Faraday collectors. ⁴⁰Ar is detected on a collector with a 10¹¹ ohm resistor, and the remaining isotopes are collected and measured on four detectors fitted with 10¹² ohm resistors (for ³⁶Ar to ³⁹Ar). The equipment is connected to a stainless steel purification line where 0.1 ml of gas is introduced and purified by cold and hot getter pumps (reactive gas removal). Measuring errors are estimated to be smaller than ±1%.

4. Results

Table 1 lists the sample locations together with the depth of the wells and the T (°C), pH, electrical conductivity (EC, in μS/cm), and oxidation-reduction potential (ORP, in mV) field data. Data for dissolved gas compositions, expressed in mlSTP_s/L_{H2O}, are presented in Table 2. Helium and C isotopic compositions and ⁴He/²⁰Ne ratios are reported in Table 3, while the available Ar isotope data (samples 11–15, 17 and 19) are listed in Table 4.

Starting from the gas-chromatographic analyses, the composition of the dissolved gas phase was calculated by combining the solubility coefficients (Bunsen coefficient “β”, ml_{gas}/L_{H2O}) of each gas species at the equilibration temperature, the volume of gas extracted (ml), and the volume of the water sample as shown in Eq. (1):

$$G_C = \left\{ \left[G_{gc} \right] * V\gamma_e + \left(\left[G_{gc} \right] * \beta_G * VW \right) \right\} VW^{-1} * V\gamma_e * V\gamma_i^{-1} / 100 \quad (1)$$

where G_C is the concentration of the selected gas specie, G_{gc} is its concentration measured by gas chromatography (vol.%), Vγ_e and Vγ_i represent the extracted and the introduced gas volumes, respectively, while VW is the volume of the analyzed water sample (see also Italiano

et al., 2009, 2013 for further details). All volumes are carefully measured at the equilibration temperature.

The analytical results of Table 2 show the presence of variable oxygen amounts in all vented thermal fluids. The N₂/O₂ ratios, often used to detect the presence of an atmospheric component, are well above (up to about 100 times) the N₂/O₂ ratio in Air Saturated Water (ASW) (4.8 mlSTP/L) in the majority of the artesian waters, except for a few samples (column 8, Table 2) that have N₂/O₂ values close to the atmospheric ratio (~2). The most abundant non-atmospheric component is CO₂, whose content is well above the equilibrium with ASW (0.24 mlSTP/L_{H2O}; Weiss, 1974) in the three basins, ranging from about 10 times (average for Millungera), to 50–200 times (for Galilee) and up to 1400 times the equilibrium value at Bonnie Doon (Cooper Basin). CH₄ is always present with concentrations ranging from 4.4 × 10⁻⁵ mlSTP/L_{H2O} at Julia Creek Railway well, and 4.9 mlSTP/L_{H2O} at Longreach. The isotopic composition of the Total Dissolved Carbon (δ¹³C TDC) ranges between -16.91 and +0.18, with different average values over the three basins (Table 3).

Samples from the Millungera Basin display negligible CH₄ content (average 5 × 10⁻² mlSTP/L_{H2O}) but are enriched in He. In contrast, volatiles from the Galilee and Cooper Basins have higher CH₄ contents (up to two orders of magnitude, on average 1.5 and 1.2 mlSTP/L_{H2O}, respectively), and differ from each other in their helium content (higher in the Cooper relative to the Galilee Basin).

Helium concentrations, well above the equilibrium with ASW (4.8 × 10⁻⁵ mlSTP/L_{H2O}), vary from about 6 × 10⁻⁴ to 1.2 × 10⁻¹ mlSTP/L_{H2O} with an isotopic signature ranging from 0.01 Ra_c to 0.1 Ra_c (where c stands for “corrected values”).

5. Discussion

5.1. Dissolved gas phase assemblage

A mixture of volatiles of different origin than the atmosphere is recognized to be a common feature at the investigated basins (Table 2). The non-atmospheric gas species, CO₂, CH₄ and He may either originate from crustal-derived products including granites, metasediments and oil reservoirs, or from mantle-derived products intruded in the crust or releasing mantle volatiles through lithospheric discontinuities.

The atmospheric contribution in terms of N₂/O₂ values (Table 2) is significantly different among the three basins, which can be roughly

Table 2
Chemical composition of the dissolved gases. Data in cc_{gas}/L_{H2O}. Columns 1–7 list the chemical composition calculated by the gas-chromatographic analyses (see text). Concentrations of reactive gases CH₄, CO and H₂ are normally negligible in non-industrial areas as expected for the Australian Outback. ASW = composition of Air Saturated Water reported for comparison.

Sample ID	Site name	Basin	1	2	3	4	5	6	7	8
			N ₂	O ₂	CO ₂	CH ₄	CO	H ₂	He	N ₂ /O ₂
1	Longford Plains	M	10.5	0.02	2.6	2.6E-02	1.70E-05	bdl	5.5E-02	559.9
2	Julia Creek/Railway	M	4.6	1.70	4.6	4.4E-05	1.84E-05	bdl	5.6E-02	2.7
3	Julia Creek/Scare-bore	M	10.2	2.35	2.4	2.1E-02	7.93E-04	3.9E-04	1.5E-02	4.4
4	Cabanda	M	16.5	1.36	1.9	4.0E-02	2.99E-05	6.1E-03	1.2E-01	12.2
5	Nelie	M	8.8	2.58	1.9	6.5E-04	2.80E-05	bdl	2.0E-03	3.4
6	Kynuna	M	16.7	1.44	14.4	1.9E-01	5.12E-04	2.8E-03	3.2E-02	11.6
7	Hughenden Shire-bore	G	17.7	0.32	1.4	7.8E-03	5.45E-04	bdl	3.7E-04	55.4
8	Hughenden Stamford	G	11.1	1.37	0.2	2.0E-04	1.34E-05	bdl	4.4E-04	8.1
11	Weston	G	15.9	3.69	13.8	4.3E-01	9.7E-04	2.2E-02	3.1E-03	4.3
14	Winton	G	7.8	2.09	5.3	2.5E-01	6.9E-04	2.5E-03	6.0E-04	3.7
15	Nuken	G	26.0	4.42	15.6	5.3E-01	2.4E-04	5.5E-04	9.2E-03	5.9
16	Longreach	G	7.0	1.46	1.9	4.9E+ 00	5.2E-06	6.3E-04	7.0E-03	4.8
17	Quilpie	G	5.0	0.04	54.9	4.5E+ 00	9.3E-04	3.2E-02	2.1E-02	119.1
12	Bonnie Doon	C	2.1	0.05	339.7	2.6E+ 00	2.9E-05	bdl	1.5E-02	43.6
13	Nockatunga	C	8.3	0.05	1.1	5.1E-01	1.0E-03	2.6E-01	2.4E-03	182.8
18	Birdsville	C	19.7	3.02	10.0	1.6E+ 00	1.0E-03	1.4E-02	1.0E-02	6.5
19	Yowah	C	8.6	0.04	2.5	1.2E-01	0.0E+ 00	4.2E-04	5.2E-03	194.3
9	Innot Hot bore		15.2	1.43	1.6	5.9E-02	1.87E-05	bdl	1.2E-01	10.6
10	Innot Hot Spring		8.2	0.12	1.1	3.7E-02	5.73E-04	1.9E-02	5.3E-02	66.2
	ASW		9.6	4.8	0.24	<1E-5	<1E-6	<1E-6	4.8E-5	2.0

Table 3

Helium to neon ratios and isotopic composition of helium and carbon. Helium isotopic compositions are reported as R/Ra values together with the measurements errors. R_{ac} stands for recalculated values after removal of atmospheric contribution following the procedure described in Hilton (1993). Only samples with ⁴He/²⁰Ne > 5 were recalculated. ⁴He/²⁰Ne = 0.267 was used as ASW reference (Holocher et al., 2002). Carbon isotopic composition is reported in ‰ against V-PDB international standard. The δ¹³C_{TDC} values are recalculated from the δ¹³C_{TDC} following Zhang et al. (1995). Typical values from natural sources are listed for comparison.

Sample ID	Basin	Site name	R/Ra	He/Ne	R/Rac	δ ¹³ C _{TDC}	δ ¹³ C _{CO2}
1	M	Longford Plains	0.03 ± 0.003	139.12	0.03	−13.70	−16.05
2	M	Julia Creek/Railway	0.03 ± 0.002	113.23	0.03	−14.62	−17.05
3	M	Julia Creek/Scare-bore	0.04 ± 0.001	58.20	0.04	−14.52	−16.91
4	M	Cabanda	0.03 ± 0.003	69.97	0.03	−14.55	−17.70
5	M	Nelie	0.12 ± 0.003	15.97	0.10	−16.86	−19.79
6	M	Kynuna	0.02 ± 0.001	41.51	0.01	−13.94	−15.39
7	G	Hughenden Shire-bore	0.21 ± 0.013	1.52	–	−16.91	−21.08
8	G	Hughenden Stamford	0.09 ± 0.011	4.09	–	−16.86	−20.70
11	G	Weston	0.12 ± 0.014	3.95	–	−12.63	−12.76
14	G	Winton	0.10 ± 0.026	16.04	0.08	−13.19	−13.43
15	G	Nuken	0.04 ± 0.007	28.24	0.03	−12.19	−11.90
16	G	Longreach	0.09 ± 0.0015	59.67	0.09	−8.70	n.d.
17	G	Quilpie	0.10 ± 0.018	35.07	0.09	−7.18	−9.23
12	C	Bonnie Doon	0.02 ± 0.0012	265.77	0.02	−5.89	−2.36
13	C	Nockatunga	0.03 ± 0.0012	171.44	0.03	0.18	−1.37
18	C	Birdsville	0.06 ± 0.0012	57.82	0.05	−6.69	−6.80
19	C	Yowah	0.06 ± 0.0013	45.59	0.05	−6.11	−8.35
9		Innot Hot bore	0.04 ± 0.004	116.21	0.04	−14.67	−15.64
10		Innot Hot Spring	0.05 ± 0.002	217.90	0.05	−14.67	−16.14
ASW			1	0.267			−7*
Volcanic fluids			2 to 7	>1000			−7 to 0
MORB			8	>1000			−6.5
Crustal fluids			0.05	>1000			−2 to 2
Radiogenic fluids			0.01	>1000			n.d.
Biogenic fluids			n.d.	n.d.			<−20

classified as air-depleted (Cooper), air-enriched (Galilee), and intermediate (Millungera). The two samples from Innot Hot Springs falling within the overlapping fields of the Millungera and Galilee Basins represent a separate group and are different from each other in their O₂ and CO₂ content.

Considering the low (and often negative) ORP values (Table 1) besides a N₂ content well above the equilibrium with ASW, the dissolved O₂ appears to be mainly due to local infiltration of shallow waters (e.g. from the periodical flooding affecting the Australian outback) and/or the consequence of contamination (due to well construction and possibly leakage) of the deep artesian groundwaters by shallow air-equilibrated waters.

The O₂–He–CO₂ triangular diagram (Fig. 2) shows the relationships between gas species typically representative of the atmosphere (O₂) and other sources (namely crust and mantle). Gas/water interaction (GWI) processes (arrows in Fig. 2) seem to be responsible for the composition of the dissolved gas assemblage: deep-originated volatiles (containing CO₂ and He) rise towards the surface, and interact with air-equilibrated groundwaters (ASW, represented by O₂ in Fig. 2). Further GWI accounts for CO₂ dissolution.

Apart from the obvious CO₂ enrichment in volcanic areas, the venting of CO₂-rich waters has been observed in geothermal areas

Table 4

Ar analyses and He concentrations expressed as 10^{−4} vol.%. ⁴⁰Ar* = Argon excess to the atmospheric in ppm by vol.; n.a. = not analyzed; n.d. = not determined. AIR: atmospheric values reported for comparison.

Sample ID	Basin	Site name	⁴ He	⁴⁰ Ar	³⁸ Ar	³⁶ Ar	⁴⁰ Ar*	⁴⁰ Ar/ ³⁶ Ar _c
11	G	Weston	76.5	12240.7	7.7	41.3	28.8	294.9
14	G	Winton	297.3	11711.6	7.4	39.7	n.d.	293.8
15	G	Nuken	559.1	8357.3	5.2	27.8	139.4	299.1
17	G	Quilpie	733.1	11057.3	7.0	37.4	14.0	294.6
12	C	Bonnie Doon	1631.0	1211.6	0.7	3.9	47.7	306.3
13	C	Nockatunga	2079.2	7668.6	4.9	26.0	n.d.	293.8
19	C	Yowah	967.0	11904.3				293.4
AIR			5.2	9780.0	6.2	33.1		295.5

well-known for their CO₂-rich thermal springs (e.g. Yellowstone, Wairakei or Larderello geothermal systems), in tectonically active continental areas (e.g. North and East Anatolian Fault Zone, Turkey Italiano et al., 2013) where CO₂-rich thermal waters bring a mixture of mantle-derived and metamorphic CO₂ (Gianelli, 1985), and in the seismically active Central Apennines (Italy) where CO₂-rich springs carry gaseous CO₂ produced by mechano-chemical reactions (Italiano et al., 2008). The CO₂ extracted from our thermal waters may have been supplied by either a crustal or a mantle source. In order to further constrain the origin of the dissolved volatiles, their carbon isotopic composition was investigated and considered together with information from the light noble gases (He, Ne, Ar).

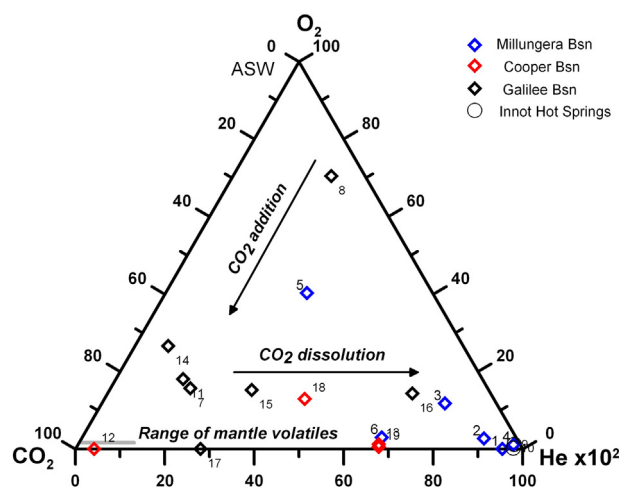


Fig. 2. Composition of the gases dissolved in the studied waters. The arrows show the trends produced by the addition and dissolution of CO₂ to an atmospheric gas assemblage (see text for details). The grey bar shows the range for mantle volatiles. ASW – Air Saturated Water. Sample symbols: blue diamonds = Millungera Basin; black diamonds = Galilee Basin; red diamonds = Cooper Basin; open black circles = Innot Hot Springs. Samples ID as reported in Tables 1–4. (For interpretation of the references to colour in this figure legend, the reader is referred to the web version of this article.)

5.2. Carbon–He–Ar systematics

5.2.1. Carbon

CO₂ is a very reactive gas with very high solubility in water. Its isotopic composition can be easily modified by a large spectrum of geochemical processes. When involved in gas/water interaction, gaseous CO₂ equilibrates isotopically with HCO₃⁻ and CO₃²⁻ ions in the aqueous phase, and the mole fraction of each species is a function of the pH of the solution. The δ¹³C_{TDC} values reported in Table 3 represent the average of the isotopic composition of the dissolved carbon species, expressed as the isotopic balance of dissolved carbon species weighted on the respective carbon contents as:

$$\delta^{13}\text{C}_{\text{TDC}} = \left(\delta^{13}\text{C}_{\text{CO}_{2\text{aq}}} * \chi_{\text{CO}_{2\text{aq}}} + \delta^{13}\text{C}_{\text{HCO}_{3}} * \chi_{\text{HCO}_{3}} \right) / M \quad (2)$$

where χ is the molar fraction and M is the total mass of dissolved carbon. CO₂(aq) and HCO₃⁻ are the predominant carbon species at the pH range (6.1–8.7, Table 1) of the sampled waters, therefore the observed δ¹³C values for dissolved inorganic carbon (δ¹³C_{TDC}) are a function of the mole fraction of HCO₃⁻.

Since GWI processes that resulted in carbon fractionation may have occurred at variable extent during gas uprising and CO₂ dissolution, we recalculated the theoretical isotopic composition of the gaseous CO₂ interacting with the groundwaters. According to Deines (1970) and Zhang et al. (1995) the δ¹³C_{CO₂aq} and δ¹³C_{HCO₃} can be computed considering the isotope enrichment factors (ϵ) for the CO₂gas–HCO₃ (ϵ_{α}) and the CO₂gas–CO₂aq (ϵ_{β}) systems. The isotopic ratio of the gaseous CO₂ can be recalculated as

$$\delta^{13}\text{C}_{\text{CO}_{2}} = \delta^{13}\text{C}_{\text{TDC}} - \left[\epsilon_{\alpha} * \chi_{\text{HCO}_{3}} + \epsilon_{\beta} \chi_{\text{CO}_{2}} \right] \quad (3)$$

The results, reported in Table 3, show how the pristine gaseous CO₂ had an isotopic signature more negative by some 2–5‰ with respect to the TDC, except for the sample from Bonnie Doon.

The δ¹³C_{CO₂} vs CO₂ content (mlSTP/L_{H₂O}) plotted in Fig. 3(a) shows two main groups, one of which includes samples from the Millungera and Galilee Basins with δ¹³C_{CO₂} values ranging from –22.72 to –10.02‰, and the other, including samples from the Cooper Basin, from –9.06 to –0.59‰. For both groups the more negative is the δ¹³C, the lower is the CO₂ content, thus representing variable extents of GWI processes. Apart from the GWI, the observed δ¹³C ranges are consistent with the presence of different CO₂ reservoirs feeding the ground waters that circulate over the studied basins, in agreement with previous studies (Boreham et al., 2001).

The natural CO₂ sources are marked by different δ¹³C ratios (δ¹³C_{MORB} = –6.5‰; δ¹³C_{Limestones} = 0‰, δ¹³C_{Marine sediments} = –20‰; Faure and Faure, 1986; Javoy et al., 1986; Sano and Marty, 1995), although mixing of volatiles from different sources and fractionation processes may produce similar δ¹³C values. The range of measured carbon isotopic compositions for TDC (–16.91‰ < δ¹³C_{TDC} < +0.18‰) and CO₂ (–21.08‰ < δ¹³C_{CO₂} < –1.37‰) allows us to exclude a main input of organic CO₂ (typically ranging from –70‰ to –25‰) to the deep gas phase. The isotopically heavy carbon (δ¹³C_{TDC} + 0.18‰, δ¹³C_{CO₂} –1.37) of Nockatunga (Cooper Basin) suggests a contribution from carbonate devolatilization, likely sourced from high-temperature water–rock interactions or from over-mature sediments (Sun, 1997; Deighton and Hill, 1998). Although any high-temperature interaction requires a thermal source (e.g. the mantle, Italiano et al., 2008), CO₂ from this site is isotopically different from those of the Cooper Basin (as well as those of the Gippsland and Bonaparte basins; Boreham et al., 2001), which are normally depleted in heavy carbon (δ¹³C < –10‰), despite the extremely high CO₂ contents. Variable degrees of degassing may account for the loss of the light (¹²C) carbon isotope from the pristine CO₂-dominated gas phase released at Nockatunga. Since Boreham et al. (2001) pointed out that gases with CO₂ contents >5% and falling in the

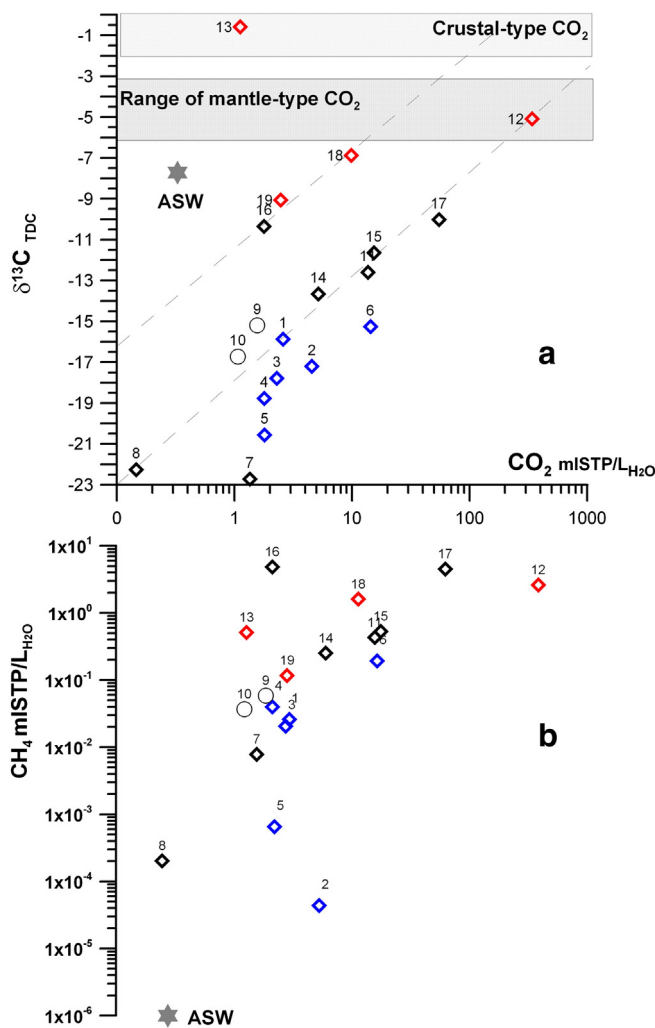


Fig. 3. a, b. CO₂ content vs (a) isotopic composition of δ¹³C_(CO₂) and (b) CH₄ concentration. The Cooper Basin broadly shows less negative δ¹³C values than the Millungera and Galilee Basins falling close to the typical values of magmatic and hydrothermal CO₂. The evident δ¹³C–CO₂ relationships account for gas–water interactions (GWI) inducing CO₂ loss and carbon fractionation. The occurrence of similar trends followed by samples from different basins suggests that the content of dissolved CO₂ is not solely controlled by interactions with groundwater, and that the coexistence of multiple sources has to be considered. (b) Shows the existence of linear relationships between CO₂ and CH₄. Sample symbols: blue diamonds = Millungera Basin; black diamonds = Galilee Basin; red diamonds = Cooper Basin; open black circles = Innot Hot Springs. Samples ID as reported in Tables 1–4. (For interpretation of the references to colour in this figure legend, the reader is referred to the web version of this article.)

range –3 < δ¹³C < –10‰ are considered to be derived from an inorganic igneous and/or mantle source (Smith and Pallasser, 1996; Pallasser, 2000), we argue that although CO₂-rich volatiles from multiple sources may feed the same basin, there is a clear contribution from the mantle either directly (volatiles degassing) or indirectly (conductive thermal energy).

Fig. 3b shows the CO₂ content against the CH₄ content. The samples fall along a broadly increasing trend for the two gas species, showing that despite the occurrence of GWI, the two gas species are closely linked together. Considering that 1) CH₄ is not a major component in mantle fluids, 2) CH₄ may be released from hydrocarbon reservoirs (Carothers and Kharaka, 1980), but in this case it would not be linearly correlated with CO₂ as shown in Fig. 3b; 3) CH₄ is abundant in geothermal reservoirs where, in the presence of water, the reactive carbon species (CH₄, CO and CO₂) equilibrate as a function of the local P–T conditions (e.g. Italiano and Nuccio, 1991; Italiano et al., 2013), we propose that geothermal systems where volatiles equilibrate during their rise towards the surface can be responsible for CH₄ production and for

the observed CO₂–CH₄ relationships. In line with this proposition, the isotopic composition of the bubbling gas from the hottest sample (Birdsville, Cooper Basin; $\delta^{13}\text{C}_{\text{CH}_4} = -45\%$ and $\delta\text{D}_{\text{CH}_4} = -175\%$) indicates a thermogenic origin for CH₄ (Schoell, 1980, 1988), and thus supports the existence of high-temperature geothermal reservoirs.

5.2.1. Helium

The ⁴He/²⁰Ne ratios (Table 3) denote a low or negligible atmospheric contribution in the sampled waters, in agreement with the chemical composition of the dissolved gases, assuming that all ²⁰Ne is of atmospheric origin.

The isotopic composition of the dissolved helium (Table 3) has been corrected for atmospheric contamination by using the air-normalized ⁴He/²⁰Ne ratio multiplied by the ratio of its Bunsen coefficient (see caption of Fig. 4). The air-corrected ³He/⁴He ratios (R/R_c) of the dissolved helium range between 0.01 and 0.1 R_c (Table 3). Most of the measured helium isotopic ratios fall within the range of crustal helium (0.02–0.05 R_c; Table 3), although the corrected ratios at Winton (0.08 R_c), Longreach (0.09 R_c) and Quilpie (0.09 R_c), all in the Galilee Basin, are higher than typical crustal values. Additional ³He inputs to the local ground waters may thus only be due to mantle-derived volatiles permeating at depth (Martel et al., 1989). It is noteworthy that the highest and the lowest ³He/⁴He values were recorded within the Millungera Basin: at Nelie (0.1 R_c) and Kynuna (0.01 R_c). The latter is consistent with the ³He/⁴He ratio expected from in situ radiogenic production in crustal lithologies (Mamyrin and Tolstikhin, 1984; Andrews, 1985; Ballentine and Burnard, 2002), while the former denotes contributions from a ³He-rich source. We argue that it would be very unlikely for ³He-rich volatiles (either from the mantle or from magmatic intrusions) to move towards the surface across the granites located at depth (Korsch et al., 2011) in the absence of active tectonic structures. Reactivation of truncated thrust faults that occur along the western and eastern margin of the Millungera Basin (Carr et al., 2010) may have facilitated the migration of ³He-rich volatiles to the surface. Recent geophysical studies show local low seismic velocity anomalies in the Millungera Basin (Saygin et al., 2013), which may be associated with fault-controlled local occurrences of mantle-derived and/or heated fluids. Indeed, the highest ³He/⁴He value (0.1 R_c) at Nelie coincides with a low seismic velocity and gravity anomaly (location 6 in Saygin et al., 2013).

MORB-like volatiles in the Australian lithospheric mantle have been revealed by the geochemical composition of the noble gases trapped in CO₂-rich fluid inclusions from southeastern Australia (Matsumoto et al., 2000; Cartwright et al., 2002), which is marked by a mean ³He/⁴He ratio of $1.1 \pm 0.2 \times 10^{-5}$, and within the range reported for MORBs ($1.2 \pm 0.1 \times 10^{-5}$; ~8 Ra; Hilton et al., 1993; Farley and Neroda, 1998; Ozima and Podosek, 2002; Graham, 2002). Mantle-type volatiles are incorporated in ground waters at Mt Gambier (up to 3 Ra; Chivas et al., 1987) and in the eastern GAB (0.81 Ra; Love et al., 2009) and western GAB (0.16 Ra at Warburton Spring, and 0.72 Ra at Bubbler Spring; Love et al., 2009). The ³He/⁴He ratios of our samples fall in the 0.01–0.1 R_c range, indicating ³He injections accompanied by significant amounts of dissolved CO₂. To evaluate the extent of mantle volatile contribution to the dissolved gas phase as well as elemental fractionations between He and CO₂, we examined the correlation between CO₂/³He and CO₂ (Fig. 4a) and between CO₂/³He and R/R_c (Fig. 4b).

CO₂/³He ratios plotted against dissolved CO₂ content describe an apparent trend (Fig. 4a) up to a maximum CO₂/³He value of 5.9×10^{11} as the CO₂ contents increase. This CO₂/³He value was recorded at Bonnie Doon (Cooper Basin), and the crustal ³He/⁴He ratio of 0.02 Ra reflects also a possible addition of ³He-depleted, CO₂-dominated volatiles potentially derived from hydrothermal devolatilization of carbonates (see $\delta^{13}\text{C}$ values in Table 3 and Fig. 3). In the plot of CO₂/³He versus R/R_c (Fig. 4b), the absence of any correlation suggests that the observed CO₂/³He ratios are not the result of simple mixing between crustal and mantle volatiles. In Fig. 4b, the crustal volatiles should

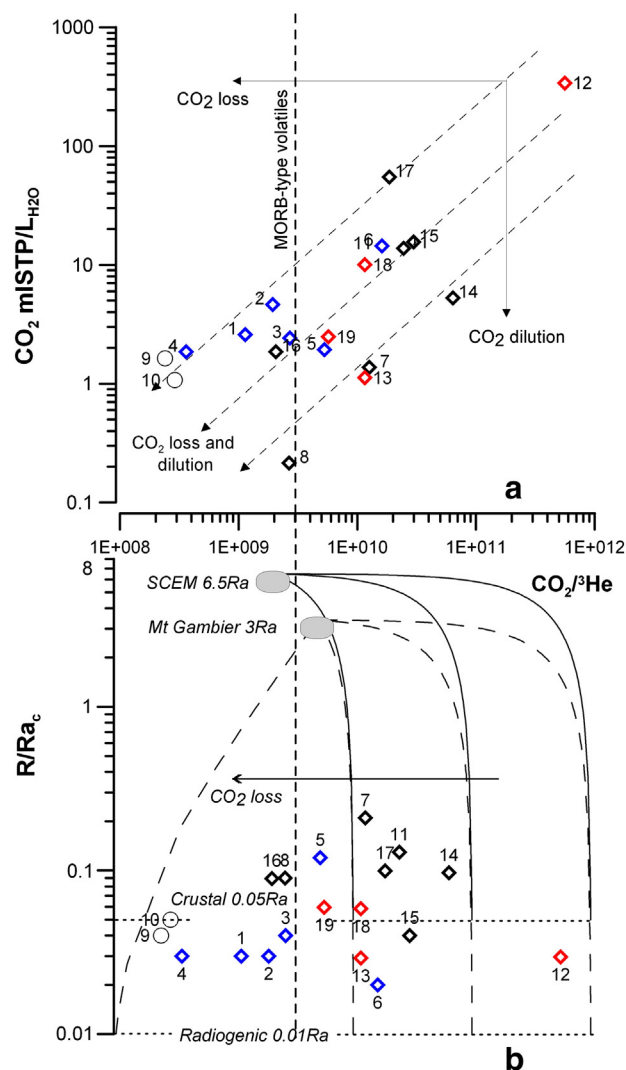


Fig. 4. CO₂–³He relationships. CO₂/³He vs CO₂ content (mLSTP/L-H₂O) (a) and (b) CO₂/³He vs ³He/⁴He (R/R_c) ratios. Sample symbols: blue diamonds = Millungera Basin; black diamonds = Galilee Basin; red diamonds = Cooper Basin; open black circles = Innot Hot Springs. Samples ID as reported in Tables 1–4. The shaded area highlights the range of pure MORB-type volatiles. The sample distribution on (a) shows trends of CO₂ dissolution at variable extents (dashed lines) with almost constant ³He contents. Figure (b) combines (a) with the information that helium isotopes do not denote simple crust/mantle mixings (see text), however variable CO₂/³He ratios at constant ³He/⁴He ratios are possible results of subsequent elemental fractionation. All error bars are within the symbols size. Mixing curves in (b) are shown for mantle end-members with 6.5 Ra (SCEM, solid lines) and 3 Ra (dashed, Mt. Gambier type volatiles; grey areas on top of the plots) with CO₂/³He in the range of 2×10^9 and 3×10^9 , and crustal end-members with 0.01 Ra (radiogenic) and 0.05 (crustal, dotted horizontal lines), and CO₂/³He ratios ranging between 10^9 and 10^{12} . $R/R_c = R/R_c$ corrected for ASW helium = $[R/R_c \cdot (X-1)] / (X-1)$ where X is the ASW-normalized ⁴He/²⁰Ne ratio taken as 0.267 (Holocher et al., 2002). (For interpretation of the references to colour in this figure legend, the reader is referred to the web version of this article.)

plot within the area defined by R/R_c of up to 0.05 and CO₂/³He ratios up to 10^{14} , however the highest ratio is lower than 10^{12} . Almost all the samples from the Galilee Basin plus two from the Cooper and one from the Millungera Basin show small but measurable additions of ³He-rich volatiles. GWI processes are responsible for the CO₂ loss that largely changes the CO₂/³He ratios, moving the samples along the trends (dotted line) shown in Fig. 4a.

The amount of helium that dissolves in the deep ground waters following GWI is a function of the molar fraction of helium in the gas phase. Since the helium molar fraction in mantle-type volatiles (in the range of $0.9\text{--}20 \times 10^{-4}$ vol.%; e.g., Fischer et al. (1998), and references therein) is 2–4 orders of magnitude lower than in crustal fluids

(3000–5000 × 10⁻⁴ vol.%; e.g., Fourré et al. (2011)), it can be expected that the dissolved crustal-derived helium be dominant when the basal flux is made of volatiles from both crustal and mantle sources.

The ⁴He/²⁰Ne vs R/Ra_c graph in Fig. 5 shows that almost all the samples fall between the mixing lines of atmosphere with upper and lower continental crust, here assumed to be carbonate-enriched (upper crust) and made of granitic and crystalline rocks (lower crust). Some helium isotope values, however, are not compatible with such a simple atmosphere–crust (either upper or lower) mixing model, suggesting contributions from a ³He-enriched source. We constructed two theoretical curves that broadly fit those values (mainly from the Galilee Basin) by adding to the upper crust, (taken as 0.05 Ra) 25% and 50% contributions of Mt Gambier-type helium (3 Ra; Love et al., 2009). The aim of Fig. 5 is not to quantify the percentage of mantle contribution to the dissolved gases, but to highlight the presence of fluids that can be considered as “intermediate” fluids carrying 2–15% mantle He (Pik and Marty, 2008) over the three investigated basins.

The data published in Torgersen et al. (1992) provide further support to the model presented here. Some of the Ra values measured in central Australia (black filled circles in Fig. 5) are similar to the values measured in this study (e.g., in Birdsville) or are even higher (0.59 Ra in Oakwood and 0.568 Ra in Juanbang). The ³He–⁴He–CO₂ ternary diagram in Fig. 6 provides further support to our findings. The sample distribution on the graph shows variable extents of CO₂ dissolution, as well as the addition of ³He. As the ³He content is calculated from the helium isotopic ratios corrected for atmospheric contamination (albeit very low or insignificant; see Table 3), the ³He addition can only have a mantle origin.

5.2.2. Argon

Due to its high solubility in water, the presence of argon in any ASW is mainly due to atmospheric contribution, thus is normally not very useful to measure Ar isotopic ratios in dissolved gases. Some samples,

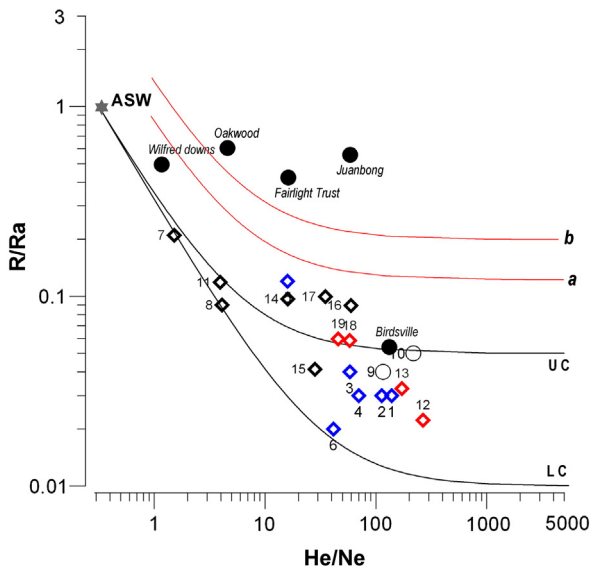


Fig. 5. He/Ne vs uncorrected R/Ra relationships of samples from this study and selected samples after Torgersen et al. (1992). The black lines represent mixings of atmospheric and crustal-type (Lower Crust – LC and Upper Crust – UC) helium. Red lines represent 25 (a) and 50% (b) admixture of subcontinental-type helium (3Ra as from Mt Gambier) to a crustal + atmosphere mixture. Assumed end-members used for the mixing lines: ASW (1 Ra, He/Ne = 0.285; Mamyrin and Tolstikhin, 1984); SCM (3Ra and He/Ne ratio = 1000; e.g. Mt. Gambier, Love et al., 2009; Czuppon et al., 2009); Upper Crust and Lower Crust are assumed to have R/Ra = 0.02 and He/Ne = 5000, and R/Ra = 0.01 and He/Ne = 5000, respectively. Error bars are smaller than the plotted symbols. Sample symbols: black filled circles = Torgersen et al., 1992; blue diamonds = Millungera Basin; black diamonds = Galilee Basin; red diamonds = Cooper Basin; open black circles = m Innot Hot Springs. Samples ID as reported in Tables 1–4. (For interpretation of the references to colour in this figure legend, the reader is referred to the web version of this article.)

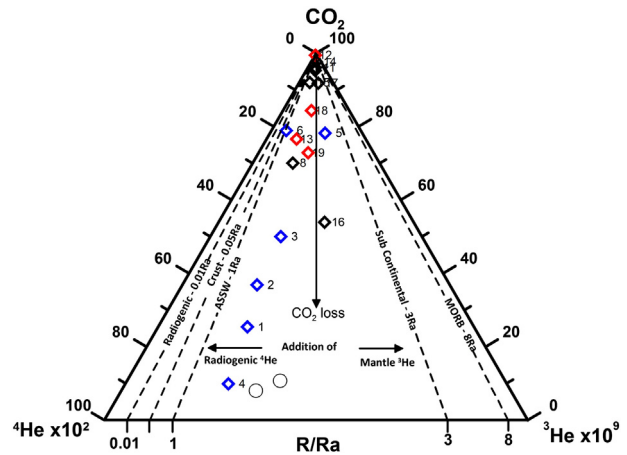


Fig. 6. ³He–⁴He–CO₂ ternary diagram. The samples are plotted with respect to relative contributions of both helium isotopes after the removal of air contamination. The dotted lines display the mixing lines between a CO₂ gas phase and helium of different origin (MORB, SCM, AIR, Crust). The effects of progressive CO₂ dissolution as well as the effects of ³He and ⁴He addition are shown by the arrows.

however, displayed free gas separated from the water inside the sealed sampling bottle, therefore they were selected for spectrometric analyses of ³⁶Ar, ⁴⁰Ar, and ⁴He concentration together with their ⁴⁰Ar/³⁶Ar isotopic composition. Helium and Ar concentrations range from 76 to >2000 × 10⁻⁴ vol.%, and from 1211 to >12,000 × 10⁻⁴ vol.%, respectively (Table 4). These values are well above the air content (5.2 and 9780 × 10⁻⁴ vol.%, respectively; Table 4) and do not represent variable extents of air contamination. The ⁴⁰Ar concentrations corrected for atmospheric contribution range from 14 to 139 ppm, suggesting a measurable argon contribution from endogenic sources, in agreement with the corrected ⁴⁰Ar/³⁶Ar isotopic ratios of up to 306.3 (Table 4). The data in Fig. 7(a, b) show two trends of crustal and mantle volatiles contributions in terms of argon versus helium isotopes, consistent with the results of the chemical and isotopic compositions of CO₂ and He.

5.3. Mantle fluid injection and the role of neotectonics

The presented geochemical features of the dissolved gases indicate multiple volatile sources including spatially variable proportions of deeply-derived (endogenic) fluids. The presence of significant amounts of CO₂, CH₄ and He with ³He/⁴He values higher than the typical range for crustal fluids of 0.02–0.05 Ra indicate that deep mantle-derived fluids can rise to the surface through the ductile lower crust and brittle upper crust. Considering the general assumption that fluid passage through the impermeable ductile lower crust is difficult (e.g. Kennedy and van Soest, 2007), the fundamental question to be dealt with is how mantle volatiles are injected into the crustal–fluid system in a continental intraplate tectonic setting.

The passage of mantle fluids through the ductile boundary can occur by mantle decompression beneath thin continental crust leading to partial melting and degassing of mantle-derived magmas (Ballentine et al., 2002b). In regions void of active or recently active volcanism, as is the case in the study area, a magmatic flow of mantle fluids through the ductile lower crust can also occur due to the creation of permeable pathways as a result of crustal deformation (Kulongoski et al., 2005; Kennedy and van Soest, 2007). Crustal deformation and the associated seismic activity in continental intraplate regions occur commonly through reactivation of pre-existing zones of weakness such as regions of extended continental crust (c.f., Johnston and Kanter, 1990; Kato et al., 2009).

Australia is the most rapidly moving continent globally, drifting north at a current speed of approximately 7 cm/year (Kennett and Blewett, 2012). The northward movement resulted in collision with Eurasia in the Timor and Papua New Guinea regions (Huston et al.,

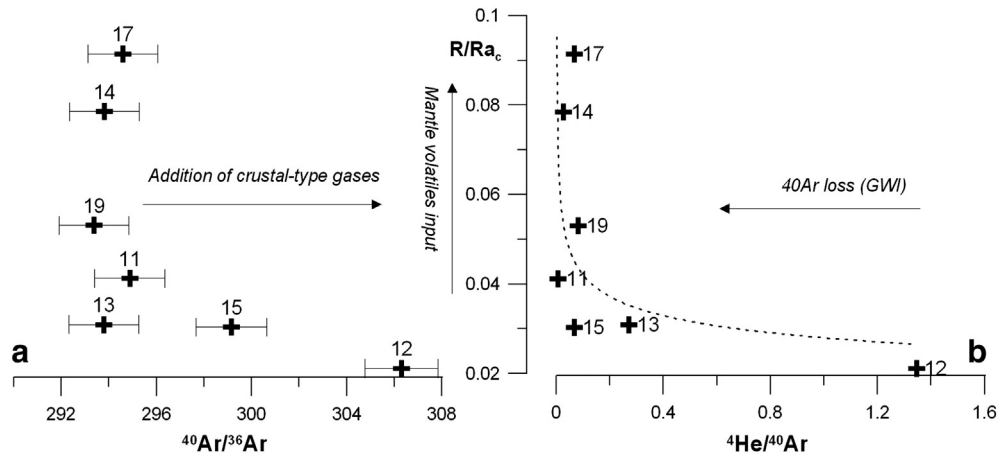


Fig. 7. (a) $^{40}\text{Ar}/^{36}\text{Ar}$ versus $^3\text{He}/^4\text{He}$ isotopic ratios, and (b) $^4\text{He}/^{40}\text{Ar}$ versus $^3\text{He}/^4\text{He}$ isotopic ratios. The arrows in figures (a) and (b) show the concomitant effects on helium and argon isotopes on the addition of crustal and mantle-type volatiles (^{40}Ar increase and R/R_{ac} decrease) and argon loss during GWI due to very high Ar solubility. Air values are shown for reference. All values are corrected for atmospheric contamination. Sample symbols: blue diamonds = Millungera Basin; black diamonds = Galilee Basin; red diamonds = Cooper Basin; open black circles = Innot Hot Springs. Samples ID as reported in Tables 1–4. (For interpretation of the references to colour in this figure legend, the reader is referred to the web version of this article.)

2012), with the plate boundary forces acting upon the Australian Plate and inducing a compressional stress regime in central and eastern Australia (Hillis and Muller, 2003). The Australian continent is thus one of the most seismically active intraplate regions in the world. A number of major recent reverse fault earthquakes involving surface fault rupture have occurred in central Australia, with many pre-historic fault scarps having been discovered (McCue, 1990). The main regions of documented neo-tectonic activity in Australia are the extended crustal areas, particularly those representing Mesozoic major rifting episodes, where normal faults have been reactivated as reverse faults under compression (Clark et al., 2011). The most prominent examples of neotectonic activity are found in South Australia in the Flinders and Mount Lofty Ranges, which are bound to the East and the West by reverse faults that thrust Proterozoic and/or Cambrian basement rocks above Quaternary sediment (Quigley et al., 2006). A number of faults have been documented in this region showing Pliocene to Quaternary displacements (see Clark et al., 2011 and references therein). Further north and closer to the study area in Queensland (Lake Eyre region), the deformation of Miocene-age sediments is the obvious consequence of neotectonic activity (Waclawik et al., 2008). A number of historical earthquakes with magnitudes between 3 and 7 have been recorded in central Australia, particularly in northern South Australia, southwest Queensland and the Northern Territory (Hillis et al., 2008; see also <http://www.quakes.uq.edu.au>). Samples with R/R_{ac} values indicating contributions of mantle volatiles seem to be located along significant fault systems and may indicate lithospheric faults. In contrast, samples (e.g. # 11, 12, and 13) with low R/R_{ac} values (crustal-type volatiles), although occurring in intensely faulted areas, may indicate the presence of shallow faults (Fig. 1).

Another indicator of neotectonic activity in the southwestern GAB is the widespread occurrence of springs and sinter deposits, which occur along faults extending from the basement to the surface (Adlam and Kuang, 1988). Some recent pilot studies have confirmed the role of neotectonics in the creation of pathways that allow the migration of deeply-sourced CO_2 -rich fluids in the groundwater system (Uysal et al., 2013). Travertine deposits in southwest Queensland and northern South Australia are particularly significant, as they form due to CO_2 degassing when the highly carbonated groundwaters emerge along faults. Some of the carbonate and silica sinter deposits in the southwestern GAB are intensely fractured and show evidence of faulting. Field observations and structural mapping near Lake Eyre showed that pre-existing faults were reactivated neotectonically and controlled the formation of late Quaternary carbonate vein and breccia deposits, which formed in hydro-fractures during the release of overpressured CO_2 -rich fluids (Uysal et al., 2013). High precision U-series dating of

carbonate veins suggests that the release of the pressurised CO_2 occurred intermittently from 35.9 ± 0.15 ka to 1.2 ± 0.02 ka (Uysal, unpublished data), possibly in association with mantle degassing in response to seismicity, analogous to similar deposits in seismically active geothermal systems worldwide (Hancock et al., 1999; Rihs et al., 2000; Chiodini et al., 2004; Newell et al., 2005; Uysal et al., 2007; Uysal et al., 2009).

5.4. Heat origin and potential for geothermal resources in the GAB

The release of mantle-derived volatiles implies a large amount of CO_2 as well as the supply of significant amounts of thermal energy to fluids located in crustal levels, including ground waters and oil reservoirs. The release of conductive thermal energy by granites at shallow crustal levels (upper crust) differs from the typically convective thermal energy of mantle origin released at the level of the lower crust (or deeper). Therefore, the new conceptual model for the GAB needs to incorporate individual sub-basins with varying chemistry, flow paths and mixing dynamics and temperature conditions.

Seismic tomography techniques have been used extensively to locate geothermal anomalies (e.g., Foley et al., 1992; Munoz et al., 2010; Saygin and Kennett, 2012; Muksin et al., 2013). Low seismic velocity anomalies in central Australia recorded by Saygin and Kennett (2010) coincide with areas where high heat flow anomalies occur (Chopra and Holgate, 2005). These regions are also defined by the thinnest crust in the Australian continent, approximately 30 km thick, in the southern extension of the study area in southwest Queensland and northeast South Australia (Kennett et al., 2011). Substantially higher heat flows (113.0 ± 2.9 mW/m² and 107.5 ± 1.7 mW/m²) have been reported further north in the Millungera Basin. These values are well above the regional average of 65–90 mW/m² (Faulkners et al., 2012; Fitzell et al., 2012), and correspond to low seismic velocity regions (Saygin et al., 2013; see also Section 5.2.1) possibly caused by higher heat production due to deep crustal fracturing and/or neotectonic fault reactivation, and hence mantle heat release at a scale smaller than the whole GAB.

6. Conclusions

Analysis of dissolved gases in artesian waters of the GAB revealed the presence of CO_2 (up to about 340 cm³ CO_2 mlSTP/L_{H₂O}) and significant amounts of helium (up to 1.2×10^{-1} mlSTP/L_{H₂O}). $\delta^{13}\text{C}_{\text{CO}_2}$ and $^3\text{He}/^4\text{He}$ as high as -1.37% and 0.1 R_{ac} , respectively, suggest the presence of a deep mantle-derived source for some of the released He and CO_2 . A mantle contribution ranging from 0.5% to 2.5% is estimated based on the $^3\text{He}/^4\text{He}$ isotope systematics of the GAB waters

investigated in this and previous studies, with the largest component inferred for the Galilee Basin.

Recent seismic tomography studies are consistent with our gas geochemistry results, suggesting that deep crustal fracturing and degassing, and hence heat released from the mantle, occur at a scale smaller than the whole GAB.

Volatiles from different sources (both shallow and deep) contribute to feed the circulating waters that move across tectonic structures and discontinuities, generating a wide array of geochemical signatures. The geochemical features of dissolved He and CO₂ are consistent with the proposed presence of mantle-derived CO₂ over the Cooper basin (Boreham et al., 2001) and the area's anomalously high heat flow (Sass and Lachenbruch, 1978; Cull and Conley, 1983; Torgersen et al., 1992; Beardsmore, 2004; Chopra and Holgate, 2005; Korsch et al., 2011). The gas geochemistry data contribute to better constrain the groundwater flow path by highlighting the geochemical variability of the vented fluids over the three investigated basins, and provide further evidence that the GAB cannot be considered as a single and relatively simple water reservoir. More detailed small-scale studies including structural mapping are needed to conclusively establish the link between faulting and mantle degassing.

Acknowledgements

This work was financially supported by the Queensland Geothermal Energy Centre of Excellence, the National Institution for Geophysics and Volcanology-INGV (Italy), the Eskisehir Osmangazi University (Turkey) (project no. 2011/15022), and the Australian National Centre for Groundwater Research and Training. Two anonymous reviewers and the editor in chief David Hilton whose comments and suggestions greatly improved the final version of the paper are kindly acknowledged. The authors wish to thank Hugh Russell and Glenda Heyde for their valuable help to carry out this project. The authors are indebted to Hal Gurgenci and Andrew Glikson for their valuable comments and suggestions. Mauro Martelli, Andrea Rizzo, Marcello Liotta and Fausto Grassa are kindly acknowledged for their support during the laboratory work.

Appendix A

A.1. Helium permeation through pyrex glass

Helium diffusion through pyrex glass is known to be a potentially serious problem for sample storage before helium isotope analysis due to the rate of helium diffusion through pyrex glass bottles (e.g. Sano and Fischer, 2012). For this reason, pyrex bottles are not commonly used for the collection of fluids/gases for helium isotope analysis. However, as optimization of sampling and analytical methods must be based on scientific evidence, all available experimental information must be considered before a certain procedure can be adopted or deemed to be unsuitable for a specific purpose. In this appendix, we review the available evidence for He diffusivity through pyrex glass, and argue that pyrex glass bottles are suitable for the sampling and storage of fluids/gases for He isotope analysis as long as the storage time does not exceed two months.

In a recent paper by Sano and Fischer (2012), the problem of long-time storage of samples for helium isotopic analysis is discussed considering the permeation constant of pyrex glass of 1.5×10^{-11} ccSTP/s/cm²/mm/Torr (at 25 °C), experimentally determined by Norton (1953). Sano and Fischer (2012) calculated a permeation rate of 3.2×10^{-6} ccSTP/day of total helium for a pyrex bottle with 280 cm² inner surface area, 0.7 mm thick glass, 300 ml internal volume, an internal helium concentration of 1.3 vol.% and atmospheric helium concentration outside the bottle ($\Delta P \approx 10$ Torr = 7.5×10^{-2} Pa). Under these conditions, it would take 10 years for the sample to equilibrate with the atmosphere. This is a short time compared to lead glass, whose permeation constant is lower by one order of magnitude

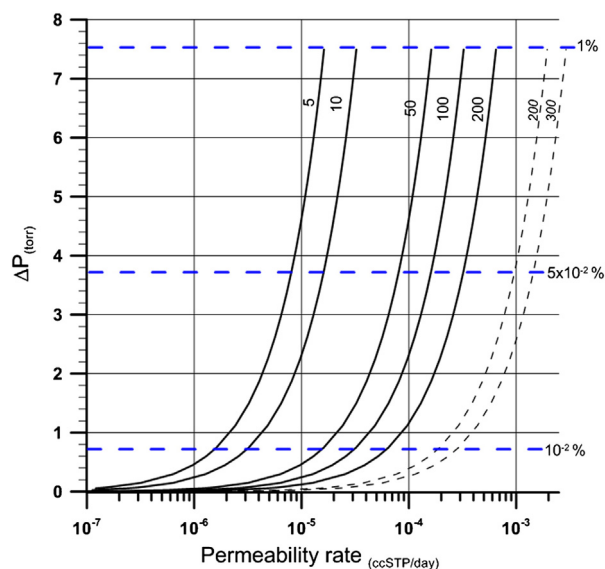


Fig. A1. Theoretical curves for helium permeability rates (PR) through pyrex glass as a function of the inside/outside pressure gradient (ΔP). The curves show the PR through surface areas in the range of ranging from 5 to 300 cm² (see labels as marked on the curves) for thicknesses of 1 and 3 mm (dashed and thick lines, respectively). Pyrex glass diffusion coefficient of 1.5×10^{-11} ccSTPs/cm²/mm/Torr (at 25 °C) after Norton (1953); pressure gradients calculated for a fixed constant external helium pressure of 5.24×10^{-4} KPa (3.93×10^{-3} Torr) and variable inside pressures for variable corresponding to helium contents in the range of 1×10^{-4} –10 KPa (4.5×10^{-3} –7.5 Torr).

(9.1×10^{-12} ccSTP/s/cm²/mm/Torr; Norton, 1953), and thus implying an equilibration time of the order of one century.

Fig. A1 shows the permeability rates as a function of the He partial pressure gradient for different surface areas and thicknesses. Considering a helium concentration inside the pyrex bottle of 100 ppm ($10^{-2}\%$), the permeability rate ranges from 1.5×10^{-6} to 3×10^{-4} ccSTP/day. The range is 1×10^{-5} to 2×10^{-3} ccSTP/day for a 1% He concentration. At this rate, a gas sample stored in our 240 ml pyrex bottles (inner surface area of 367 cm² and 3 mm wall thickness) will take about 10 years to equilibrate with the atmospheric helium concentration, almost

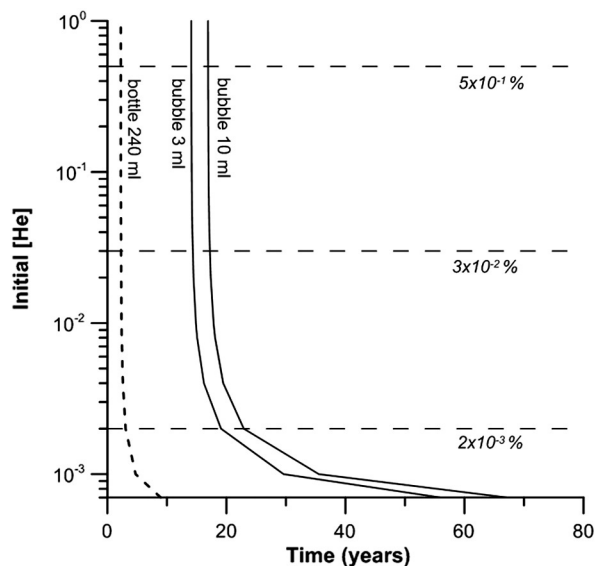


Fig. A2. Full equilibration time between internal and external helium partial pressure (namely sample-atmosphere) as a function of the initial helium content in the range $1-10^4$ ppm (10^{-2} –1%) for gas bubble bottle volumes of 3, 10 and 240 (gas-filled bottle) ml. The relatively fast helium permeation through pyrex glass doesn't allow long-term laboratory gas samples storage. The water samples for dissolved gas analysis can be stored for a longer time represent a different case due to the small or negligible volumes of free gas (exsolved gas bubbles) in contact with the pyrex glass walls.

irrespective of the initial He concentration within the range 100 ppm to 1% (Fig. A2).

Since the permeability rates are direct and linear functions of surface area, time and concentration gradient, and inverse function of thickness, a decrease in helium concentration by an order of magnitude leads to an equilibration time of one millennium for leaded glass. Therefore, a storage time of up to 2–3 years in leaded glass will not compromise the sample's integrity (Sano and Fischer, 2012).

A.2. The case of water samples for dissolved gas analyses

Water samples collected for dissolved gas analyses typically require further laboratory procedures for gas extraction. The sampling bottles are not filled with gas, and therefore the pyrex glass surface area through which helium can permeate is not the whole inner surface area of the bottle, but only that of the gas bubble formed by gas exsolution and/or water

volume contraction due to cooling. For example, for a 240 ml water sample collected at 85 °C, a temperature drop of 60 °C to room temperature (assumed to be 25 °C) generates a volume contraction of 3.024 ml (estimated considering the volumetric expansion relationship for liquids $\Delta V = KV_0\Delta T$, where K = volumetric thermal expansion coefficient for water = $2.14 \times 10^{-4} \text{ } ^\circ\text{C}^{-1}$ and for $V_0 = 240 \text{ ml}$), which creates a bubble that is filled with gases exsolved from the water. Helium can diffuse from this bubble through the glass, but the permeability rate is a function of surface area and thickness of the wall, as well as helium concentration gradient. Under these conditions, the equilibration time between the sample helium and atmospheric helium becomes much longer because of the small exchange surface, although it might also be shorter due to the low amount of helium contained in the gas bubble.

Fig. A2 shows three time-dependent trends for the full equilibration of sample helium (inside) with the atmosphere (outside), calculated for gas sample volumes of 3, 10 and 240 ml (representative for bubbles generated by temperature drops of 25 and 60 °C and for a gas-filled bottle, respectively). The horizontal lines highlight the initial sample helium contents of 0.5, 0.03 and 0.002% (ranges recorded in our sample set). The relatively wide concentration range considered in these calculations also takes into account the helium enrichment in the separated gas phase due to its low solubility in the water phase. It is straightforward to observe that gas in a completely-filled bottle takes a relatively short time to equilibrate with the atmosphere (about 10 years for the considered range of helium contents). In contrast, the gas bubbles need 5 times (or even) longer to equilibrate with the atmosphere due to their reduced exchange surface areas (even considering the maximum spherical section). The conclusion of our calculations is that a long-term storage cannot be considered a reliable procedure for gas samples collected in pyrex bottles; however, it is suitable for water samples as long as the storage time does not exceed a few months.

Samples collected in pyrex bottles for this study were analyzed within 2 to 4 weeks from the date of sampling. The first batch was sampled between 5 and 11 November 2011, and the second from 13 to 16 December 2011. All samples were shipped to Italy by fast cargo and were analyzed on 25 November 2011 (first batch) and 9–10 January 2012 (second batch). The maximum He loss within this time frame would be 0.3% (for a large-size bubble with the highest helium content of 0.5% by volume) of the initial content (Fig. A3a,b). For these reasons,

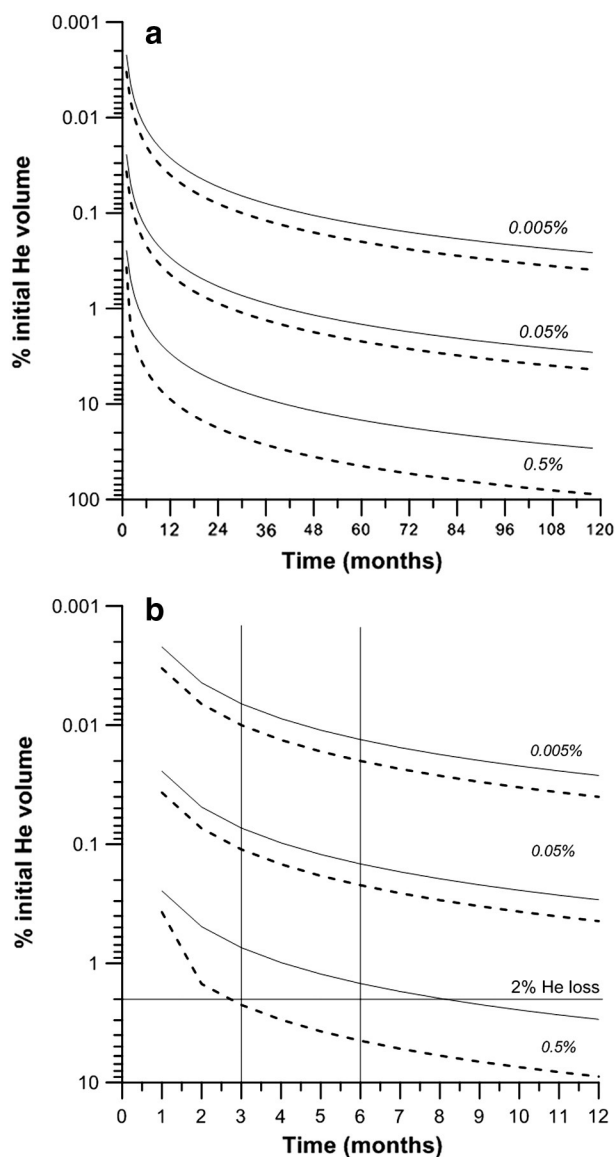


Fig. A3. a) Percentage of helium loss as a function of time on a time scale of 10 years as a function of the initial helium content. Three examples are shown for gas bubbles of 5 and 10 cm³ (dashed and solid lines, respectively) with initial helium contents of 0.005, 0.05 and 0.5% by volume. b) Detail of Fig. A3a with a time scale of 1 year, showing that storage times shorter than 12 months do not impact on the integrity of the sample for helium concentrations as high as 0.05%. Higher helium contents require a shorter storage time (e.g., for 0.5% [He] and a gas bubble of 5 cm³ in a 240 ml pyrex glass bottle, a storage time of 3 months would result in a helium loss as high as 2%).

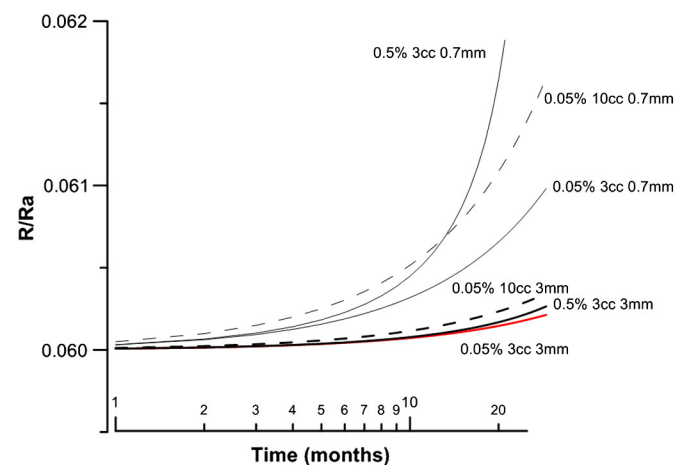


Fig. A4. The plot shows the temporal changes in helium isotopic ratio as a function of the initial helium concentration (here assumed to be 0.5 and 0.05% by volume), the volume of the bubble (10 and 3 cc) and the thickness (0.7 and 3 mm) of the pyrex wall, over a time span of 2 years. All trends are simulated for an initial isotopic ratio of 0.06 Ra. The red line refers to the sample from the Birdsville well. All simulations show that it is possible to preserve the helium isotopic ratio of the samples over a relatively long time span, as the changes in R/Ra values are smaller than the analytical error ($\pm 2\%$). In our case, changes in the isotopic composition lag behind changes in the concentration (see Fig. 3a,b). (For interpretation of the references to colour in this figure legend, the reader is referred to the web version of this article.)

Table A1

Comparison of the Birdsville artesian bore data after Torgersen (1992) and our study (this work). We noted a lower temperature (by 10 °C) and He/Ne ratio compared to Torgersen et al. (1992) but a higher helium concentration.

BIRDSVILLE	Bore N°	Longitude	Latitude	T°C	R/Ra	He/Ne	R/Rac	[He] ccSTP/L
This work	14,645	25° 51'44"	139° 28'22"	87	0.06 ± 0.0012	57.8	0.05	1 × 10 ⁻²
Torgersen et al. (1992)	14,645	-25.8966	139.3519	97	0.0696	129	0.05	4.68 × 10 ⁻³

we consider the ³He/⁴He values reported in Table 3 as representative of the waters sampled.

Helium isotopes can be fractionated during helium permeation because of the different diffusivity of masses 3 and 4. Following Trull and Kurz (1999), low isotopic diffusivity ratios ($D^3\text{He}/D^4\text{He}$) require significantly large He losses to alter initial ³He/⁴He ratios. Considering a $D^3\text{He}/D^4\text{He} = 1.15$ (at room temperature – from Graham's Law), the initial ³He/⁴He ratio may be lowered by 10% for a 65% He loss. This value increases to 80% for a diffusivity ratio of 1.08 (Trull and Kurz, 1999). Considering that the helium loss from our samples is always below 0.5% (even in the worst-case scenario of 0.5% initial He content – see Fig. A3b), the resulting isotopic fractionation is negligible and within the measurement error.

Further simulation tests have been carried out to evaluate the temporal changes in isotopic ratio due to the simultaneous ⁴He-loss/³He-gain through the pyrex walls induced by the different pressure gradients of the two isotopes. Fig. A4 shows the simulations for 0.7 and 3 mm pyrex glass wall thicknesses with internal helium contents of 0.5 and 0.05%. The ³He partial pressure in the dissolved gas sample is calculated from the helium content, the total gas content and the gas/water partition coefficient as a function of temperature. For example, the "Birdsville" sample (³He/⁴He ratio = 0.06 Ra) has a helium content of 1 × 10⁻² ccSTP/L and a total gas content of 35.36 ccSTP/L (Table 2). These values yield a ³He partial pressure of 9.86 × 10⁻⁸ hPa, which is an order of magnitude higher than the atmosphere (7.28 × 10⁻⁹ hPa). This ³He pressure, always higher than the atmosphere, prevents atmospheric ³He permeation and isotopic fractionation as a function of sample storage time. As a result of the above calculations and considerations, we recommend that samples collected in pyrex glass bottles for dissolved helium analyses must be measured within 3–6 months (depending on their original helium content) from the date of collection. We further note that pyrex glass bottles are not suitable for the long-term storage of water samples because of potential helium leakage through the rubber septum. To avoid atmospheric helium diffusion through the septum, we kept the bottles upside down and with the necks submerged in salty water even during sample shipping and laboratory handling.

The measured helium isotopic ratios in this work, well below the atmospheric value, are consistent with a lack of atmospheric contamination due to ³He permeation through the pyrex or the septum as a consequence of the large ³He partial pressure difference between air and the sample. The results obtained in previous studies using the same sampling equipment and methods (e.g., Italiano et al., 2013 and references therein) show that these precautions make our methodology suitable for the analytical determinations of all dissolved gases (including all the main gases, noble gases and their isotopic composition, and total dissolved carbon isotopes).

To conclude, although no duplicate samples were collected by using different containers, we note that the helium isotopic ratio measured in a sample from the Birdsville well (Table A1) collected in copper tubes by Torgersen et al. (1992) and our sample collected 20 years later from the same well but using a pyrex bottle are virtually identical.

References

Adlam, R., Kuang, K.S., 1988. An investigation of structures controlling discharge of spring waters in the south western Great Artesian Basin. Department of Mines and Energy, South Australia, Adelaide.

- Andrews, J.N., 1985. The isotopic composition of radiogenic He and its use to study groundwater movement in confined aquifer. *Chemical Geology* 49, 339–351.
- Ballentine, C.J., Burnard, P.G., 2002. Production, release and transport of noble gases in the continental crust. In: Porcelli, D., Ballentine, C.J., Wieler, R. (Eds.), *Rev. Mineral. Geochem.* 47. Mineral. Soc. of Am., Washington, D. C., pp. 481–538.
- Ballentine, C.J., Burgess, R., Marty, B., 2002b. Tracing fluid origin, transport and interaction in the crust. In: Porcelli, D., Ballentine, C.J., Wieler, R. (Eds.), *vol. 47. Mineral. Soc. of Am., Washington, D. C.*, pp. 539–614.
- Banerjee, A., Person, M., Hofstra, A., Sweetkind, D., Cohen, D., Sabin, A., Unruh, J., Zvyolovski, G., Gable, C.W., Crossey, L., Karlstrom, K., 2011. Deep Permeable Fault-Controlled Helium Transport and Limited Mantle Flux in Two Extensional Geothermal Systems in the Great Basin, USA. *Geology* 39, 195–198.
- Beardsmore, G., 2004. The influence of basement on surface heat flow in the Cooper Basin. *Explor. Geophys.* 35, 223–235.
- Bethke, C.M., Zhao, X., Torgersen, T., 1999. Groundwater flow and the ⁴He distribution in the Great Artesian Basin of Australia. *J. Geophys. Res.* 104 (B6), 12,999–13,011.
- Boreham, C.J., Hope, J.M., Hartung-Kagi, B., 2001. Understanding source, distribution and preservation of Australian natural gas: a geochemical perspective. *APEA J.* 2001, 523–547.
- Carothers, W.W., Kharaka, Y.K., 1980. Stable isotopes of HCO₃ in oil field waters implications for the origin of CO₂. *Geochim. Cosmochim. Acta* 44, 323–332.
- Carr, L.K., Korsch, R.J., Jones, L.E.A., Holzschuh, J., 2010. The role of deep seismic reflection data in understanding the architecture and petroleum potential of Australia's onshore sedimentary basins. *APPEA, Journal and Conference Proceedings* 50, 4.
- Cartwright, I., Weaver, T., Tweed, S., Ahearne, D., Cooper, M., Czapnik, K., Tranter, J., 2002. Stable isotope geochemistry of cold CO₂-bearing mineral spring waters, Daylesford, Victoria, Australia: sources of gas and water and links with waning volcanism. *Chem. Geol.* 185, 71–91.
- Chiodini, G., Cardellini, C., Amato, A., Boschi, E., Caliro, S., Frondini, F., Ventura, G., 2004. Carbon dioxide Earth degassing and seismogenesis in central and southern Italy. *Geophys. Res. Lett.* 31, L07615.
- Chivas, A.R., Barnes, I., Evans, W.C., Lupton, J.E., Stone, J.O., 1987. Liquid carbon dioxide of magmatic origin and its role in volcanic eruptions. *Nature* 326 (6113), 587–589.
- Chopra, P., 2003. Preview Australian Society of Exploration Geophysics 107, 34–36.
- Chopra, P.N., Holgate, F., 2005. A GIS analysis of temperature in the Australian crust. *Proceedings World Geothermal Congress 2005. Antalya, Turkey, 24–29 April 2005* (7 pp.).
- Clark, D., McPherson, A., Collins, C.D.N., 2011. Australia's seismogenic neotectonic record: a case for heterogeneous intraplate deformation. *Geoscience Australia, Record 2011/11* (95 pp.).
- Commonwealth of Australia, 2010. OzTemp-Interpreted Temperature at 5 km depth. Geoscience Australia (<https://www.ga.gov.au/products/servlet>).
- Cull, J.P., Conley, D., 1983. Geothermal gradients and heat flow in Australian sedimentary basins. *BMR J. Aust. Geol. Geophys.* 8, 329–337.
- Czuppon, G., Matsumoto, T., Handler, M.R., Matsuda, J.I., 2009. Noble gases in spinel peridotite xenoliths from Mt Quincan, North Queensland, Australia: undisturbed MORB-type noble gases in the subcontinental lithospheric mantle. *Chem. Geol.* 266, 19–28.
- Deighton, I., Hill, A.J., 1998. Thermal and burial history. In: Gravestock, D.I., Hibbert, J.E., Drexel, J.F. (Eds.), *Petroleum Geology of South Australia. Vol. 4-Cooper Basin*. Department of Primary Industries and Resources, Government of South Australia, pp. 143–155.
- Deines, P., 1970. The carbon and oxygen isotopic composition of carbonates from the Oka Carbonatite complex, Quebec, Canada. *Geochim. Cosmochim. Acta* 34, 1199–1225.
- Duncan, R.A., McDougall, I., 1989. Time-space relationships for Cainozoic intraplate volcanism in eastern Australia, the Tasman Sea and New Zealand. In: Johnson, J.W. (Ed.), *Intraplate Volcanism in Eastern Australia and New Zealand*. Cambridge University Press, Cambridge, pp. 43–53.
- Farley, K.A., Neroda, E., 1998. Noble gases in the Earth's Mantle. *Annu. Rev. Earth Planet. Sci.* 26, 189–218.
- Faulkners, P., Maxwell, M., O'Connor, L.K., Sargents, S.N., 2012. Coastal Geothermal Energy Initiative GSQ Julia Creek 1: well completion report and heat flow modelling results. *Queensland Geological Record*, 2012/05.
- Faure, G., Faure, G., 1986. *Principles of Isotope Geology*, 2nd edition. Wiley, New York p. 589.
- Fischer, T.P., Giggenbach, W.F., Sano, Y., Williams, S.N., 1998. Fluxes and sources of volatiles discharged from Kudryavy, a subduction zone volcano, Kurile Islands. *Earth Planet. Sci. Lett.* 160, 81–96.
- Fitzell, M.J., Maxwell, M., O'Connor, L.K., Sargent, S.N., Talebi, B., 2012. Coastal Geothermal Energy Initiative GSQ Dobbyn 2: well completion report and heat flow modelling results. *Queensland Geological Record*, 2012/04.
- Foley, J.E., Toksoz, M.N., Batini, F., 1992. Inversion of teleseismic travel time residuals for velocity structure in the Larderello Geothermal Field, Italy. *Geophys. Res. Lett.* 19, 5–8.
- Fouéré, E., Di Napoli, R., Aiuppa, A., Parello, F., Gaubi, E., Jean-Baptiste, P., Allard, P., Calabrese, S., Ben Mamou, A., 2011. Regional variations in the chemical and helium-carbon isotope composition of geothermal fluids across Tunisia. *Chem. Geol.* 288, 67–85.

- Gianelli, G., 1985. On the origin of geothermal CO₂ by metamorphic processes. *Boll. Soc. Geol. Ital.* 104, 575–584.
- Graham, D.W., 2002. Noble gas isotope geochemistry of mid-ocean ridge and ocean island basalts: characterization of mantle source reservoirs. In: Porcelli, D., Ballentine, C.J., Wieler, R. (Eds.), *Rev. Mineral. Geochem.*, 47. Mineral. Soc. of Am, Washington, D. C., pp. 247–317.
- Güleç, N., Hilton, D.R., Mutlu, H., 2002. Helium isotope variations in Turkey: relations to tectonics, volcanism and recent seismic activities. *Chemical Geology* 187, 129–142.
- Habermehl, M.A., 2001. Wire-line logged waterbores in the Great Artesian Basin, Australia – Digital data of logs and waterbore data acquired by AGSO. AGSO Bull., 245. Bureau of Rural Sciences Publication, Canberra, Australia.
- Habermehl, R., Pestov, I., 2002. Geothermal Resources of the Great Artesian Basin, Australia. *GHC Bull.* (20–26).
- Hancock, P.L., Chalmers, R.M.L., Altunel, E., Cakir, Z., 1999. Travtonics: using travertines in active fault studies. *J. Struct. Geol.* 21 (8–9), 903–916.
- Heeswijck, A.V., 2006. The structure, sedimentology, sequence stratigraphy and tectonics of the northern Drummond and Galilee Basins, central Queensland, Australia. PhD Thesis Earth Environ. Sci., vol. 1. James Cook University p. 156.
- Hillis, R.R., Müller, R.D., 2003. Evolution and Dynamics of the Australian Plate. *Geological Society of America, Boulder*, ISBN: 0-8137-2372-8 363.
- Hillis, R.R., Sandiford, M., Reynolds, S.D., Quigley, M.C., 2008. Present-day stress, seismicity and Neogene-to-Recent tectonics of Australia's 'passive' margins: intraplate deformation controlled by plate boundary forces. In: Johnson, H., Doré, A.G., Gatliff, R.W., Holdsworth, R., Lundin, E.R., Ritchie, J.D. (Eds.), *The nature and origin of compression in passive margins*. *Geol. Soc. Lond. Spec. Publ.*, vol. 306, pp. 71–90.
- Hilton, D.R., Hammerschmidt, K., Loock, G., Friedrichsen, H., 1993. Helium and Argon Isotope Systematics of the Central Lau Basin and Valu Fa Ridge: Evidence of Crust/Mantle Interactions in a Back-arc Basin. *Geochim. Cosmochim. Acta* 57, 2819–2841.
- Hilton, D.R., 1996. The helium and carbon isotope systematics of a continental geothermal system: results from monitoring studies at Long Valley caldera (California, U.S.A.). *Chemical Geology* 127 (4), 269–295.
- Holocher, J., Peeters, F., Aeschbach-Hertig, W., Hofer, M., Brennwald, M., Kinzelbach, W., Kipfer, R., 2002. Experimental investigations on the formation of excess air in quasi-saturated porous media. *Geochim. Cosmochim. Acta* 66 (23), 4103–4117.
- Huston, D.L., Blewett, R.S., Champion, D.C., 2012. The evolution of the Australian continent. *Episodes* 35, 23–44.
- Italiano, F., Nuccio, P.M., 1991. Geochemical investigations on submarine volcanic exhalations to the East of Panarea, Aeolian Islands. *Italy. Jour. Volc. And Geoth. Res.* 46, 125–141.
- Italiano, F., Martelli, M., Martinelli, G., Nuccio, P.M., 2000. Geochemical evidences of melt intrusions along lithospheric faults of Irpinian Apennines (Southern Italy): geodynamic and seismogenetic implications. *J. Geophys. Res.* 105 (B6), 13569–13578.
- Italiano, F., Martinelli, G., Nuccio, P.M., 2001. Anomalies of mantle-derived helium during the 1997–1998 seismic swarm of Umbria-Marche, Italy. *Geophys. Res. Lett.* 28 (5), 839–842.
- Italiano, F., Martinelli, G., Plescia, P., 2008. CO₂ degassing over seismic areas: the role of mechanochemical production at the study case of Central Apennines. *Pure Appl. Geophys.* 165 (1), 75–94.
- Italiano, F., Bonfanti, P., Ditta, M., Petrini, R., Slejko, F., 2009. Helium and carbon isotopes in the dissolved gases of Friuli region (NE Italy): geochemical evidence of CO₂ production and degassing over a seismically active area. *Chem. Geol.* 266, 76–85.
- Italiano, F., Sasmaz, A., Yuce, G., Okan, O., 2013. Thermal fluids along the East Anatolian Fault Zone (EAFZ): geochemical features and relationships with the tectonic setting. *Chem. Geol.* 339, 103–114. <http://dx.doi.org/10.1016/j.chemgeo.2012.07.027>.
- Javoy, M., Pineau, F., Delorme, H., 1986. Carbon and nitrogen isotopes in the mantle. *Chem. Geol.* 57 (1–2), 41–62.
- Johnson, R.W., 1989. *Intraplate Volcanism in Eastern Australia and New Zealand*: Cambridge University Press, Cambridge. p. 395.
- Johnston, A.C., Kanter, L.R., 1990. Earthquakes in Stable Continental Crust. *Sci. Amer.* 262, 68–75.
- Jones, J.G., Veewers, J.J., 1983. Mesozoic origins and antecedents of Australian's Eastern Highlands. *Journal of the Geological Society of Australia* 30, 305–322.
- Kato, A., Kurashimo, E., Igarashi, T., Sakai, S., Iidaka, T., Shinohara, M., Kanazawa, T., Yamada, T., Hirata, N., Iwasaki, T., 2009. Reactivation of ancient rift systems triggers devastating intraplate earthquakes. *Geophys. Res. Lett.* 36, L05301. <http://dx.doi.org/10.1029/2008GL036450>.
- Kennedy, B.M., van Soest, M.C., 2006. A helium isotope perspective on the Dixie Valley, Nevada, hydrothermal system. *Geothermics* 35, 26–43.
- Kennedy, B.M., van Soest, M.C., 2007. Flow of mantle fluids through the ductile lower crust: Helium isotope trends. *Science* 318, 1433–1436. <http://dx.doi.org/10.1126/science.1147537>.
- Kennett, B.L.N., Blewett, R., 2012. Lithospheric framework of Australia. *Episodes* 35, 9–22.
- Kennett, B.L.N., Salmon, M., Saygin, E., AusMoho Working Group, 2011. AusMoho: the variation in Moho depth in Australia. *Geophys. J. Int.* 187, 946–958.
- Korsch, R.J., Struckmeyer, H.I.M., Kirky, A., Hutton, L.J., Carr, L.K., Hoffmann, K.L., Chopping, R., Roy, I.G., Fittell, M., Totterdell, J.M., Nicoll, M.G., Talebi, B., 2011. Energy potential of the Millungera Basin, a newly discovered basin in North Queensland. *APEA J.* 295–332.
- Kulongoski, J.T., Hilton, D.R., Izbicki, J.A., 2005. Source and movement of helium in the eastern Morongo groundwater Basin: the influence of regional tectonics on crustal and mantle helium fluxes. *Geochim. Cosmochim. Acta* 69, 3857–3872.
- Langford, R.P., Wilford, G.E., Truswell, E.M., Isern, A.R., 1995. *Palaeogeographic atlas of Australia*. Volume 10–Cainozoic. Canberra, Australian Geological Survey Organisation.
- Love, A., Crossey, L., Karlstrom, K., Hilton, D.R., Wolaver, B.D., Rousseau-Gueutin, P., 2009. Toward a new paradigm for the Great Artesian Basin: hydrologic mixing, partitioned sub basins, and mantle influences on groundwater quality. *Geol. Soc. Am. Abstr. Programs* 41 (7), 28.
- Mamyryn, B.A., Tolstikhin, I.N., 1984. *Helium Isotopes in Nature*. Elsevier, New York.
- Martel, D.J., Deak, J., Dovenyi, P., Horvath, F., O'Nions, R.K., Oxburgh, E.R., Stegena, L., Stute, M., 1989. Leakage of helium from the Pannonian Basin. *Nature* 342, 21–28.
- Matsumoto, T., Honda, M., McDougall, I., O'Reilly, S.Y., Norman, M., Yaxley, G., 2000. Noble gases in pyroxenites and metasomatised peridotites from the Newer Volcanics, southeastern Australia: implications for mantle metasomatism. *Chem. Geol.* 168, 49–73.
- McCue, 1990. Australia's large earthquakes and recent fault scarps. *J. Struct. Geol.* 12, 761–766.
- Meixner, T.J., Gunn, P.J., Boucher, R.K., Yeats, A.N., Murray, L., Yeats, T.N., Richardson, L.M., Freares, R.A., 2000. South Australia. *Explor. Geophys.* 31, 24–32.
- Muksin, U., Bauer, K., Haberland, C., 2013. Seismic Vp and Vp/Vs structure of the geothermal area around Tarutung (North Sumatra, Indonesia) derived from local earthquake tomography. *J. Volcanol. Geotherm. Res.* 260, 27–42.
- Munoz, G., Bauer, K., Moeck, I., Schulze, A., Ritter, O., 2010. Exploring the Groß Schönebeck (Germany) geothermal site using a statistical joint interpretation of magnetotelluric and seismic tomography models. *Geothermics* 39 (1), 35–45.
- Newell, D.L., Crossey, L.J., Karlstrom, K.E., Fischer, T.P., Hilton, D.R., 2005. Continental-scale links between the mantle and groundwater systems of the western United States: evidence from travertine springs and regional He isotope data. *GSA Today* 15, 4–10.
- Norton, F.J., 1953. Helium diffusion through glass. *J. Am. Ceram. Soc.* 36, 90–96. <http://dx.doi.org/10.1111/j.1151-2916>.
- Ozima, M., Podosek, F.A., 2002. *Noble Gas Geochemistry*, 2nd ed. Cambridge University Press (286 pp.).
- Oxburgh, E.R., O'Nions, R.K., 1987. Helium loss, tectonics and the terrestrial heat budget. *Science* 237, 1583–1588.
- Pallasser, R.J., 2000. Recognising biodegradation in gas/oil accumulations through the $\delta^{13}\text{C}$ composition of gas components. *Org. Geochem.* 31, 1363–1373.
- Pik, R., Marty, B., 2008. Helium isotopic signature of modern and fossil fluids associated with the Corinth rift fault zone (Greece): implication for fault connectivity in the lower crust. *Chem. Geol.* 266, 67–75.
- Quigley, C., Cupperm, L., Sandiford, M., 2006. Quaternary faults of south-central Australia: palaeoseismicity, slip rates and origin. *Australian Journal of Earth Sciences* 53, 285–301.
- Radke, B., 2009. Hydrocarbon and geothermal prospectivity of sedimentary basins in Central Australia Warburton, Cooper, Pedirka, Galilee, Simpson and Eromanga Basins. *Geoscience Australia Record* 2009/25.
- Rihs, S., Condomines, M., Poidevin, J.L., 2000. Long-term behavior of continental hydrothermal systems: U-series study of hydrothermal carbonates from the French Massif Central (Allier Valley). *Geochim. Cosmochim. Acta* 64 (18), 3189–3199.
- Radke, B.M., Ferguson, J., Cresswell, R.G., Ransley, T.R., Habermehl, M.A., 2000. *Hydrochemistry and Applied Hydrodynamics of the Cadna-owie-Hooray Aquifer, Great Artesian Basin, Australia*, Bureau of Rural Sciences publication, Canberra, Commonwealth of Australia ISBN: 0 642 475547.
- Sano, Y., Fischer, T.P., 2012. The analysis and interpretation of noble gases in modern hydrothermal systems. In: Burnard, P. (Ed.), *The Noble Gases as Geochemical Tracers*, pp. 249–318.
- Sano, Y., Marty, B., 1995. Origin of carbon in fumarolic gas from island arc. *Chem. Geol.* 119, 265–274.
- Sano, Y., Wakita, H., 1988. Precise measurement of helium isotopes in terrestrial gases. *B. Chem. Soc. Jpn.* 61, 1153–1157.
- Sass, J.H., Lachenbruch, A.H., 1978. *Thermal Regime of the Australian Continental Crust, The Earth: Its Origin, Structure and Evolution*. Academic Press pp. 301–351.
- Saygin, E., Kennett, B.L.N., 2010. Ambient noise tomography for the Australian Continent. *Tectonophysics* 481, 116–125.
- Saygin, E., Kennett, B.L.N., 2012. Crustal structure of Australia from ambient seismic noise tomography. *J. Geophys. Res.* 117, B01304. <http://dx.doi.org/10.1029/2011JB008403>.
- Saygin, E., McQueen, H., Hutton, L., Kennett, B.L.N., Lister, G., 2013. Structure of Mt Isa and surroundings from seismic ambient noise tomography. *Aust. J. Earth Sci.* 60, 707–718.
- Schoell, M., 1980. The hydrogen and carbon isotopic composition of methane from natural gases of various origins. *Geochim. Cosmochim. Acta* 44, 649–661.
- Schoell, M., 1988. Multiple origins of methane in the earth. *Chem. Geol.* 71, 1–10.
- Smith, J.W., Pallasser, R.J., 1996. Microbiological origin of Australian coalbed methane. *AAPG Bull.* 80, 891–897.
- Sun, X., 1997. Structural style of the Warburton Basin and control in the Cooper and Eromanga Basins, South Australia. *Explor. Geophys.* 28, 333–339.
- Torgersen, T., Clarke, W.B., 1985. Helium accumulation in groundwater, I: an evaluation of sources and the continental flux of crustal ⁴He in the Great Artesian Basin, Australia. *Geochim. Cosmochim. Acta* 49, 1211–1218.
- Torgersen, T., Habermehl, M.A., Clarke, W.B., 1992. Crustal helium fluxes and heat flow in the Great Artesian Basin, Australia. *Chem. Geol.* 102, 139–152.
- Torgersen, T., Clarke, W.B., Habermehl, M.A., 1987. Helium isotopic evidence for recent subcrustal volcanism in eastern Australia. *Geophys. Res. Lett.* 14, 1215–1218.
- Trull, T.W., Kurz, M.D., 1999. Isotopic fractionation accompanying helium diffusion in basaltic glass. *J. Mol. Struct.* 485/486, 555–567.
- Uysal, I.T., Feng, Y., Zhao, J.X., Altunel, E., Weatherley, D., Karabacak, V., Genç, O., Golding, S.D., Lawrence, M.G., Collerson, K.D., 2007. U-series dating and geochemical tracing of late Quaternary travertine in co-seismic fissures. *Earth Planet. Sci. Lett.* 257 (3–4), 450–462.
- Uysal, I.T., Feng, Y., Zhao, J.X., Isik, V., Nuriel, P., Golding, S.D., 2009. Hydrothermal CO₂ degassing in seismically active zones during the late Quaternary. *Chem. Geol.* 265, 442–454.

- Uysal, I.T., Middleton, A.W., Ring, U., 2013. Understanding the active tectonics in Australia: implications of geothermal resources. *Proceedings Australian Geothermal Energy Conferences 2013 Brisbane, Australia*, 14–15 November 2013, pp. 99–101.
- Vasconcelos, P.M., Knesel, K.M., Cohen, B.E., Heim, J.A., 2008. Geochronology of the Australian Cenozoic: a history of tectonic and igneous activity, weathering, erosion, and sedimentation. *Aust. J. Earth Sci.* 55, 865–914.
- Waclawik, V.G., Lang, S.C., Krapf, C.B.E., 2008. Fluvial response to tectonic activity in an intra-continental dryland setting: The Neales River, Lake Eyre, Central Australia. *Geomorphology* 102, 179–188.
- Wellman, P., McDougall, I., 1974. Cainozoic igneous activity in eastern Australia. *Tectonophysics* 23, 49–65.
- Wellman, P., 1987. Eastern highlands of Australia: their uplift and erosion. *BMR Journal of Australian Geology and Geophysics* 10, 277–286.
- Weiss, R.F., 1974. Carbon dioxide in water and seawater: the solubility of a non-ideal gas. *Marine Chemistry*. 2, 203–215. [http://dx.doi.org/10.1016/0304-4203\(74\)90015-2](http://dx.doi.org/10.1016/0304-4203(74)90015-2).
- Wyborn, D., de Graaf, L., Davidson, S., Hann, S., 2004. Eastern Australian Basins Symposium II, PESA Special Publication, 423–430.
- Zhang, J., Quay, P.D., Wilbur, D.O., 1995. Carbon isotope fractionation during gas–water exchange and dissolution of CO₂. *Geochem. Cosmet. Acta* 59 (1), 107–114.